AD-A176 546 NUMERICAL STUDY OF THREE-DIMENSIONAL LAMINAR AND TURBULENT FLOWS WITH SYS (U) SCIENTIFIC RESEARCH ASSOCIATES INC GLASTONBURY CT W R BRILEY ET AL. DEC 86 1/1

UNCLASSIFIED ARO-19149.2-EG-S DAAG29-82-C-0021 F/G 20/4 NL

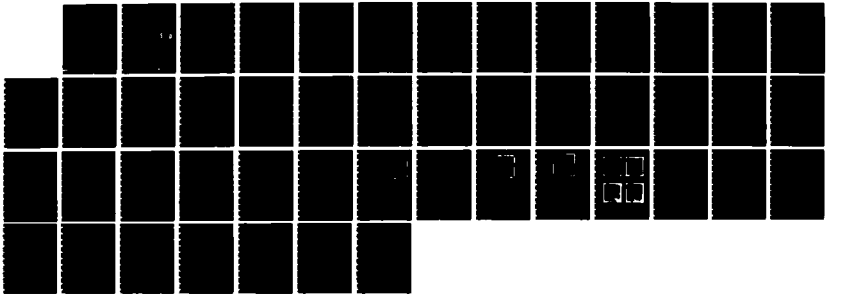

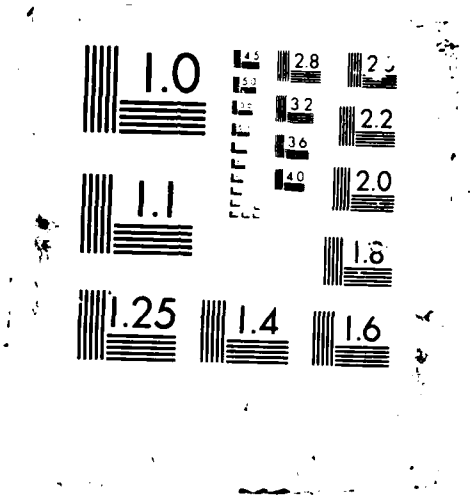
1.0
1.1
1.25
1.4
1.6
2.8
3.2
3.6
4.0
2.2
2.0
1.8

NUMERICAL STUDY OF THREE-DIMENSIONAL LAMINAR AND TURBULENT FLOWS WITH SYSTEM ROTATION

Final Report

W.R. Briley, T.R. Govindan, R. Levy and H. McDonald

DECEMBER 1986

U.S. ARMY RESEARCH OFFICE
CONTRACT DAAG29-82-C-0021

Scientific Research Associates, Inc.
Glastonbury, CT 06033

MASTER COPY - FOR REPRODUCTION PURPOSES

UNCLASSIFIED
SECURITY CLASSIFICATION OF THIS PAGE (When Data Entered)

ADA176546

REPORT DOCUMENTATION PAGE		READ INSTRUCTIONS BEFORE COMPLETING FORM
1. REPORT NUMBER ARO 19149.2-EG-S	2. GOVT ACCESSION NO. N/A	3. RECIPIENT'S CATALOG NUMBER N/A
4. TITLE (and Subtitle) Numerical Study of Three-Dimensional Laminar and Turbulent Flows with System Rotation		5. TYPE OF REPORT & PERIOD COVERED Final Report 1982-1986 6. PERFORMING ORG. REPORT NUMBER
7. AUTHOR(s) W.R. Briley, T.R. Govindan and H. McDonald		8. CONTRACT OR GRANT NUMBER(s) DAAG29-82-C-0021
9. PERFORMING ORGANIZATION NAME AND ADDRESS Scientific Research Associates, Inc. P.O. Box 1058 Glastonbury, CT 06033		10. PROGRAM ELEMENT, PROJECT, TASK AREA & WORK UNIT NUMBERS
11. CONTROLLING OFFICE NAME AND ADDRESS U. S. Army Research Office Post Office Box 12211 Research Triangle Park, NC 27709		12. REPORT DATE December 1986 13. NUMBER OF PAGES 41
14. MONITORING AGENCY NAME & ADDRESS (if different from Controlling Office)		15. SECURITY CLASS. (of this report) Unclassified 15a. DECLASSIFICATION/DOWNGRADING SCHEDULE

16. DISTRIBUTION STATEMENT (of this Report)

Approved for public release; distribution unlimited.

17. DISTRIBUTION STATEMENT (of the abstract entered in Block 20, if different from Report)

NA

18. SUPPLEMENTARY NOTES

The view, opinions, and/or findings contained in this report are those of the author(s) and should not be construed as an official Department of the Army position, policy, or decision, unless so designated by other documentation.

19. KEY WORDS (Continue on reverse side if necessary and identify by block number)

Rotating Flow;
Viscous Flow;
Parabolic Flow Analysis; Dig[illegible]

20. ABSTRACT (Continue on reverse side if necessary and identify by block number)

The spatial marching analysis is given for economical computation of three-dimensional viscous subsonic flows in rotating geometries. The governing equations are based on a small scalar potential approximation for the vector-decomposed secondary flow velocity. No approximation is needed for the streamwise pressure gradient term and this allows strong viscous secondary flows, coordinate curvature and system rotation effects to influence these pressure gradients. This approach is applied to three-dimensional laminar and

DD FORM 1 JAN 73 1473 EDITION OF 1 NOV 65 IS OBSOLETE

UNCLASSIFIED
SECURITY CLASSIFICATION OF THIS PAGE (When Data Entered)

turbulent flows in rotating 90 degree bends and in rotating straight pipes and ducts. The predicted structure of these flows is consistent with experimental observations and measurements. Computer solutions obtained using 500,000 grid points require only about 15 minutes of CRAY-1S run time. This approach appears promising for further development and application to centrifugal impeller and other turbomachinery flows.

TABLE OF CONTENTS

LIST OF FIGURES

ABSTRACT

A spatial marching analysis is given for economical computation of three-dimensional viscous subsonic flows in rotating geometries. The governing equations are based on a small scalar potential approximation for the vector-decomposed secondary flow velocity. No approximation is needed for the streamwise pressure gradient term and this allows strong viscous secondary flows, coordinate curvature and system rotation effects to influence these pressure gradients. This approach is applied to three-dimensional laminar and turbulent flows in rotating 90 degree bends and in rotating straight pipes and ducts. The predicted structure of these flows is consistent with experimental observations and measurements. Computer solutions obtained using 500,000 grid points require only about 15 minutes of CRAY-1S run time. This approach appears promising for further development and application to centrifugal impeller and other turbomachinery flows.

INTRODUCTION

The influence of system rotation on turbulent internal flows is known to have a major effect on turbomachinery performance, yet the phenomenon is poorly understood. Although used fairly extensively, centrifugal machines have in the past been designed largely on an empirical basis. In support of the empirical approach, the acquisition of experimental data from actual machines has been quite extensive. However, few fundamental experiments designed to isolate various rotation effects have been performed and consequently the understanding of the fundamental fluid mechanics of centrifugal devices is still rather sparse. The objective of the present investigation is to develop an economical method for computing three-dimensional viscous flows with system rotation, whose use will enhance the understanding and allow prediction of important physical effects of rotating flow in centrifugal turbomachines.

The extreme complexity of most turbulent rotating flows presents an obstacle for the utilization of computational methods. Such flows are three-dimensional and characterized by large secondary vorticity and velocity generated by turning and Coriolis effects, turbulent shear layers, tip clearance effects and other multiple length scale flow structures. Solution of the three-dimensional

averaged Navier-Stokes equations avoids making physical approximations other than those associated with turbulence modeling. However, this approach is very costly, even with modern supercomputers, because the flow structures of practical interest are very complicated and accurate resolution of these flow structures is expected to require very large mesh densities. To avoid this high cost of solution, physical/mathematical approximations have been developed which reduce the steady subsonic Navier-Stokes equation to a non-elliptic form which is well-posed for solution as a spatial forward-marching initial/boundary-value problem. The advantage of such an approach is that forward-marching solution algorithms can be devised which are much less costly in terms of computer resources (run time and storage) than algorithms for the elliptic Navier-Stokes equations. The trade-offs are that (a) additional error due to the physical/mathematical approximations are introduced, and (b) the range of flow problems which can realistically be addressed is restricted relative to the Navier-Stokes equations because of factors such as flow separation, stagnation points and transonic effects. Nevertheless, this approach seems well suited for a number of rotating internal ducted flows at or near design conditions, and can provide very high resolution of three-dimensional viscous flow structures at relatively low cost. In addition, the spatial marching approach can provide a large number of detailed flow calculations at moderate cost, for use in design optimization studies.

Two basic types of physical/mathematical approximations have been suggested to reduce the Navier-Stokes equations to a non-elliptic form well-posed for forward-marching solution. Approximations in both viscous and inviscid terms in the Navier-Stokes equations are necessary to obtain non-elliptic (well-posed) approximating equations. First, a coordinate system for flow geometry being considered must be constructed such that streamwise (marching) coordinates can be identified. The viscous approximation entails neglecting terms representing streamwise diffusion. In addition, two types of inviscid approximations have been suggested: (a) an assumed form for the streamwise pressure gradient term, and (b) a small scalar potential approximation for the secondary flow. Either of these approximations produces non-elliptic governing equations.

The inviscid approximation which assumes a given form for the streamwise pressure gradient term has obvious roots in two-dimensional boundary layer theory, and has been used extensively. Variants of this approach have been used, for example, by Patankar and Spalding [Ref. 1], Carreto, Curr and Spalding

[Ref. 2], Briley [Ref. 3], Ghia and Sokhey [Ref. 4], Kreskovsky, Briley and McDonald [Ref. 5] and Levy, Briley and McDonald [Ref. 6] to compute flow without system rotation and by Howard, Patankar and Bordynuik [Ref. 7] and Majumdar, Pratap and Spalding [Ref. 8] to compute flows with system rotation. Although the approximation of streamwise pressure gradients can provide reasonable accuracy for many problems, this type of approximation does not allow the streamwise momentum equation to be influenced by experimentally observed distortions of the static pressure field which are induced by large secondary flows associated with duct curvature and system rotation.

A second type of inviscid approximation (termed the small-scalar potential approximation) has been investigated recently by Briley and McDonald (Ref. 9). This approximation does not employ an approximation for streamwise pressure gradient terms and instead approximates convective terms in the secondary-flow momentum equations by neglecting the scalar-potential component of a vector-decomposed secondary-flow velocity field which corrects the transverse velocity vector from an a priori potential flow solution. This approximation allows strong viscous secondary flows and curvature terms to influence streamwise pressure gradients in the primary flow momentum equation. It should be noted that the small scalar approximation is especially advantageous for rotating flows because such flows are generally rotational even when inviscid, and this precludes any convenient method of introducing an inviscid pressure approximation, such as imposing streamwise pressure gradients from a potential flow.

In the present report, a derivation of the approximating small scalar potential equations is given for a rotating coordinate system. Computed results for three-dimensional viscous flow in simple confined rotating geometries are given. Some results for laminar flow in a rotating 90 degree bend and for turbulent flow in rotating straight ducts, previously reported by Lin, Briley and McDonald (Ref. 10) are included as part of the present final report. In addition, computed results for turbulent flow in a rotating 90 degree bend are given.

ANALYSIS

The small scalar-potential approximation is considered in detail for non-rotating coordinate systems in Ref. 9. The present analysis considers the

derivation of the applicable approximating equations for a rotating coordinate system. The governing equations are derived through approximations made relative to a curvilinear orthogonal coordinate system fitted to and aligned with the flow geometry under consideration.

Equations governing the primary flow velocity, Up, and a secondary flow vorticity, $\bar{\Omega}$, normal to the transverse coordinate surfaces are derived utilizing approximations which permit solution of the equations as an initial-value problem. Terms representing diffusion normal to the transverse coordinate planes are neglected. The contribution of scalar-potential components of secondary velocities in convective terms of the cross flow momentum equations is assumed small and is neglected. No approximation is made for pressure gradient terms, and the static pressure field is determined as part of the forward-marching solution process. Secondary-flow velocities are determined from scalar and vector potential calculations in transverse coordinate surfaces once the primary velocity and secondary vorticity are known.

Compressible Navier-Stokes Equations in Rotating Coordinate System

The continuity and momentum equations for steady compressible flow relative to rotating coordinate system in vector forms are given by

$$\nabla \cdot \rho \bar{U} = 0 \tag{1}$$

$$\rho \bar{M} = \rho \left\{ \left[(\bar{U} \cdot \nabla) \bar{U} \right] + \rho^{-1} \nabla p - \bar{F} + 2(\bar{\omega} \times \bar{U}) + \bar{\omega} \times (\bar{\omega} \times \bar{r}) \right\} = 0 \tag{2}$$

where ρ is density and $\bar{U}$ is velocity relative to rotating coordinate system. p denotes pressure and $\bar{F}$ denotes force due to viscous stress. $\bar{\omega}$ is the system rotation vector, $\bar{r}$ is the position vector. The equation of state for a perfect gas is given by

$$p = \rho RT \tag{3}$$

where R is gas constant and T is temperature. In the present study, the flows are low Mach number subsonic flows with neglible heat transfer, so the

stagnation energy can be assumed to be a known constant, E_0, and the energy equation can be omitted from consideration. For constant stagnation energy, the gas law can be written as

$$p = \frac{\gamma-1}{\gamma}\rho\left(E_0 - U\cdot\frac{U}{2}\right) \tag{4}$$

where γ is the specific heat ratio.

In the following, coordinates x,y,z, velocity components u,v,w and the unit vectors $\hat{i}_1,\hat{i}_2,\hat{i}_3$, in the x-, y- and z- directions, respectively, refer to a general rotating orthogonal coordinate system. The metric coefficients are denoted h_1, h_2 and h_3.

Secondary Velocity Decomposition

The analysis is based on a decomposition of the secondary velocity vector into vector components derived from scalar and vector surface potentials, denoted ϕ and ψ, respectively. The velocity vector is written as

$$\bar{U} = \hat{i}_1 u + \bar{U}_s \tag{5}$$

where u is the primary velocity and $\bar{U}_S$ denotes the secondary velocity. The secondary velocity is written as

$$\bar{U} = \hat{i}_2 v + \hat{i}_3 w \tag{6}$$

and is decomposed as follows:

$$\bar{U}_s = \nabla_s\phi + \frac{\rho_0}{\rho}\nabla\times\hat{i}_1\psi \tag{7}$$

Here, ∇_S is the transverse surface gradient operator, given for orthogonal coordinates by

$$\nabla_s = \hat{i}_2\frac{1}{h_2}\frac{\partial}{\partial y} + \hat{i}_3\frac{1}{h_3}\frac{\partial}{\partial z} \tag{8}$$

The transverse velocity components can be expressed as

$$v = v_\phi + v_\psi, \quad w = w_\phi + w_\psi \tag{9}$$

using (7), (8), (9), the decomposed transverse velocity components are given in orthogonal coordinates by

$$v = v_\phi + v_\psi = \frac{1}{h_2}\frac{\partial \phi}{\partial y} + \frac{1}{h_1 h_3}\frac{1}{\rho}\frac{\partial h_1 \psi}{\partial z} \tag{10a}$$

$$w = w_\phi + w_\psi = \frac{1}{h_3}\frac{\partial \phi}{\partial z} - \frac{1}{h_1 h_2}\frac{1}{\rho}\frac{\partial h_1 \psi}{\partial y} \tag{10b}$$

The decomposition of secondary velocity v, w into v_ϕ, v_ψ, w_ϕ, w_ψ, introduces two additional dependent variables and thus requires two additional equations to close the set of governing equations. The additional equations are obtained from vector identities associated with the decomposition, as discussed later.

Physical Approximations

Inviscid Approximations for Convective Terms

For convenience in defining the present approximations, a parameter, β, (to be assigned a value of 0 or 1) is introduced in the expressions for transverse velocity components as follows,

$$v = v_\phi + v_\psi, \quad \tilde{v} = \beta v_\phi + v_\psi \tag{11}$$

$$w = w_\phi + w_\psi, \quad \tilde{w} = \beta w_\phi + w_\psi \tag{12}$$

The parameter, β, will be used to define approximations in the convective terms.

Using (11) and (12), the components of the convective term $C(\Pi) \equiv (\Pi \cdot \nabla)\Pi$ can be expressed in orthogonal coordinates as follows:

$$C_1 = U\cdot\nabla u + u(vK_{12} + wK_{13}) - v^2K_{21} - w^2K_{31} \tag{13}$$

$$\tilde{C}_2 = U\cdot\nabla\tilde{v} - u(uK_{12} - \tilde{v}K_{21}) - w(\tilde{w}K_{32} - \tilde{v}K_{23}) \tag{14}$$

$$\tilde{C}_3 = U\cdot\nabla\tilde{w} - u(uK_{13} - \tilde{w}K_{31}) + v(\tilde{w}K_{32} - \tilde{v}K_{23}) \tag{15}$$

where the quantities K_{ij} are the geodesic curvatures of the coordinates, defined by

$$K_{ij} \equiv (h_i h_j)^{-1}\frac{\partial h_i}{\partial x_j} \tag{16}$$

and in which x_1,x_2,x_3 are interchangeable with x,y,z, respectively. The small scalar-potential approximation is made by setting $\beta=0$ in (11) and (12) and hence, in $\tilde{C}_2,\tilde{C}_3$; no approximation is made in C_1. If $\beta=1$, then $\tilde{v},\tilde{w}=v,w$, and the above expressions for $\tilde{C}_2,\tilde{C}_3$ revert to C_2,C_3, their exact forms.

Viscous Approximation Neglecting Streamwise Diffusion

The viscous force, F, in (2) can be written as

$$\rho F = -\nabla\times(\mu\bar{\Omega}) + (\lambda+2\mu)\nabla(\nabla\cdot\bar{U}) \tag{17}$$

where $\bar{\Omega}\equiv\nabla\times\bar{U}$ is vorticity and μ and λ are viscosity coefficients. For moderate subsonic Mach number $\nabla\cdot U$ is small, and the last term in (17) is neglected. All viscous terms which contain either a derivative with respect to x or those containing v_ϕ or w_ϕ are of smaller order than remaining terms and are neglected. Neglecting these terms give the following approximations:

For the viscous force F_1'

$$(h_1h_2h_3)\rho F_1' = \left[\frac{\partial}{\partial y}\frac{h_1^2h_3\mu}{h_2}\frac{\partial}{\partial y}\left(\frac{u}{h_1}\right) + \mu h_1^2h_3K_{12}\frac{\partial}{\partial y}\left(\frac{u}{h_1}\right)\right.$$
$$\left. + \frac{\partial}{\partial z}\frac{h_1^2h_2\mu}{h_3}\frac{\partial}{\partial z}\left(\frac{u}{h_1}\right) + \mu h_1^2h_2K_{13}\frac{\partial}{\partial z}\left(\frac{u}{h_1}\right)\right] \tag{18}$$

and for the transverse components of viscous force F_2', F_3':

$$(h_1 h_3)\,\rho F_2' = -\frac{\partial(h_1 \mu \Omega_1)}{\partial z} \tag{19a}$$

$$(h_1 h_2)\,\rho F_3' = -\frac{\partial(h_1 \mu \Omega_1)}{\partial y} \tag{19b}$$

where the streamwise vorticity is given by

$$\Omega_1 = (h_2 h_3)^{-1}\left[\frac{\partial(h_3 w_\psi)}{\partial y} - \frac{\partial(h_2 v_\psi)}{\partial z}\right] \tag{20}$$

System of Approximating Equations

Introducing the inviscid approximation for convective terms and the viscous approximation neglecting streamwise diffusion, and combining equations (2), (13), (14), (15), (18), (19) and (20), the compressible Navier-Stokes equations can be approximated as:

$$\rho M_1 = \rho\left\{C_1 + (\rho h_1)^{-1}\frac{\partial p}{\partial x} - F_1' + 2(\bar{w}\times\bar{v})_1 + \left[\bar{w}\times(\bar{w}\times\bar{r})\right]_1\right\} = 0 \tag{21}$$

$$\rho M_2 = \rho\left\{\tilde{C}_2 + (\rho h_2)^{-1}\frac{\partial p}{\partial x} - F_2' + 2(\bar{w}\times\bar{v})_2 + \left[\bar{w}\times(\bar{w}\times\bar{r})\right]_2\right\} = 0 \tag{22}$$

$$\rho M_3 = \rho\left\{\tilde{C}_3 + (\rho h_3)^{-1}\frac{\partial p}{\partial x} - F_3' + 2(\bar{w}\times\bar{v})_3 + \left[\bar{w}\times(\bar{w}\times\bar{r})\right]_3\right\} = 0 \tag{23}$$

The continuity equation and equation of state, i.e., Eqs. (1) and (4) remain unapproximated, and the decomposed secondary velocities $\bar{U}_\phi$ and $\bar{U}_\psi$ satisfy following relations

$$\hat{i}_1 \cdot (\nabla\times\bar{U}_\phi) = 0 \tag{24a}$$

$$\nabla\cdot(\rho\bar{\mathbf{w}}_{\psi}) = 0 \tag{24b}$$

The above seven equations provide a system of equations governing the five velocity components u, v_ϕ, w_ϕ, v_ψ, w_ψ, pressure p and density ρ.

Approximate Equations as a Well-Posed Initial Value Problem

It was shown in Ref. 9 that for nonrotating coordinates the foregoing approximations produce a system of equations which is well-posed. In rotating coordinates, the equations differ only in the appearance of centrifugal and Coriolis terms. These terms do not affect the well-posedness of the equations, and consequently, the system of equations (1), (4), (21), (22), (23), (24a) and (24b) is well-posed for solution as an initial/boundary value problem.

Approximate Equations Written in New Dependent Variables

Although the dependent variables and the approximate equations given above are convenient for the analysis, they are not convenient for numerical solution. The equations are reformulated for numerical solution in terms of the axial velocity, u, pressure, p, streamwise vorticity, Ω_1, scalar and vector surface potentials, ϕ and ψ, together with density, ρ. The equations for Ω_1 and p are derived by taking the divergence and curl of the transverse vector momentum equations (22) and (23). Let $M_s = \hat{i}_2 M_2 + \hat{i}_3 M_3$ denote the vector transverse momentum equation, the equations governing streamwise vorticity, Ω_1, and pressure, p, are given by

$$\hat{i}\cdot(\nabla\times\rho\mathbf{M}_s) = 0 \tag{25}$$

$$\nabla\cdot(\rho\mathbf{M}_s) = 0 \tag{26}$$

Incorporating the definition of $\bar{\Pi}_\phi$ and $\bar{\Pi}_\psi$, the continuity equation (1) becomes

$$\nabla\cdot\rho(\hat{i}u + \nabla_s\phi) = 0 \tag{27}$$

and the definition of Ω_1 becomes

$$\Omega_1 = \hat{i}_1 \cdot \nabla \times (\rho^{-1} \nabla \times i_1 \psi) \tag{28}$$

The final system of equations consists of equations (25), (26), (27) and (28) above, the x momentum equation (21), the state equation (4) for the dependent variables u, p, Ω_1, ϕ, ψ and ρ. These equations are given for a general rotating orthogonal coordinate system in Appendix A.

Turbulence Model

In turbulent flow calculations, an isotropic eddy-viscosity formulation is used for Reynolds stresses as follows:

$$\rho \overline{u_i' u_j'} = - \mu_T \frac{\partial v_j}{\partial x_i} \tag{29}$$

and the effective turbulent viscosity, μ_T, is added to the laminar viscosity, μ. The turbulent viscosity is related to mean flow variables by means of a mixing length distribution

$$\mu_T = \rho \ell_o^2 (2\bar{\bar{e}} : \bar{\bar{e}})^{1/2} \tag{30}$$

where $\bar{\bar{e}}$ is the mean flow rate of strain tensor

$$\bar{\bar{e}} = \frac{1}{2} \left[(\nabla \bar{v}) + (\nabla \bar{v})^T \right] \tag{31}$$

The mixing length, ℓ_o, is determined from the empirical relationship of McDonald and Camarata [Ref. 11] for equilibrium turbulent boundary layers which can be written

$$\ell_o(\tilde{y}) = 0.09 \delta_b \tanh \left[\frac{\kappa \tilde{y}}{0.09 \delta_b} \right] \cdot \mathcal{D} \tag{32}$$

where δ_b is the local boundary layer thickness, κ is the von Karman constant,

taken as 0.43, $\tilde{y}$ is distance from the wall, and $\mathcal{D}$ is a sublayer damping factor defined by

$$\mathcal{D} = P^{1/2}(y^+ - \bar{y}^+)/\sigma \tag{33}$$

where P is the normal probability function, $y^+ = \tilde{y}(\tau/\rho)^{1/2}/(\mu/\rho)$, τ is local shear stress, $\bar{y}^+ = 23$, and $\sigma_1 = 8$. $\tilde{y}$ is taken as the distance to the nearest wall.

It is recognized that this treatment represents a major simplification of the representation of the turbulent transport in a rotating system. However, it is also recognized that turbulent transport effects are most significant near the solid wall, and in this area a length scale varying with distance from the wall provides a reasonable first-order estimate. Further from the wall, this length scale variation becomes inaccurate, but here the flow is essentially inviscid and the errors in the length scale specification appear less important. At present, in addition to turbulence model considerations, there are major issues in adequately representing the convective processes and in obtaining accurate numerical solutions of the governing system. As a consequence, the present simple turbulence model was considered a reasonable starting point for the present turbulent work.

Numerical Method

The governing equations are replaced by an implicit finite-difference approximation. Three-point central-difference formulas are used for all transverse spatial derivatives. An analytical coordinate transformation devised by Roberts [Ref. 22] is employed for each transverse coordinate direction, as a means of introducing a nonuniform grid to concentrate grid points in the wall shear-layer regions. Two-point backward difference approximations are used for streamwise derivatives, although this is not essential.

In all the solutions reported here, no-slip or symmetry boundary conditions are prescribed, as appropriate. No boundary condition is required for density, since it is computed algebraically from the state equation. The no-slip condition, $v = w = 0$, must be expressed in terms of ϕ, ψ and Ω_1. The normal velocity component is specified by prescribing $\psi = 0$ and the Neumann condition

component of the no-slip condition is written as

$$\hat{i}_t \cdot (\bar{U}_s + \nabla_s \phi + \rho^{-1} \nabla \times \hat{i}_1 \psi) = 0 \qquad (34)$$

where $\hat{i}_t$ denotes the unit tangent vector, and the finite-difference forms of (28) and (34) are combined to provide a boundary condition relating Ω_1 at wall to ϕ and ψ. A Neumann boundary condition for pressure, p, at a no-slip wall is obtained from the normal momentum equation as

$$\hat{i}_n \cdot \left[\nabla p - \rho F' + \rho \bar{w} \times (\bar{w} \times \bar{r})\right] = 0 \qquad (35)$$

where the convective terms and Coriolis force term vanish because $\bar{U} = 0$. It is beneficial to introduce a further change of variables expressing the pressure, p, as

$$p = P(x, y, z) + p_m(x) + \Delta p(x,y,z) \qquad (36)$$

where P(x,y,z) is the potential pressure. Equation (26) now governs Δp, but does not contain p_m, which is in effect the arbitrary constant of the Neumann problem for Δp at each x-location. As a consequence, equation (26) can be solved for Δp before p_m is known, and p_m can then be adjusted during solution of the x-momentum equation to ensure that the integral mass-flux relation

$$\int (\rho u)\, dA = Q = \text{constant} \qquad (37)$$

is satisfied, where A denotes cross section area.

A summary of the procedure used to advance the solution a single streamwise step to the (n+1)-level x^{n+1} from known quantities at x^n follows. Unless specifically mentioned to the contrary, the transverse velocities v_ϕ, w_ϕ, v_ψ, w_ψ and the density ρ are evaluated explicitly at the n-level. In addition, the convective operator is evaluated as $\rho^{n} \bar{w}^{n} \cdot \nabla$. Values of $\bar{\omega}$, h_1, h_2, and h_3 are given and thus known at both x^n and x^{n+1}.

1. Equations (A.1) and (A.2) form a linear coupled system for Ω_1^{n+1} and ψ^{n+1} which is solved as a 2×2 coupled system. For this purpose artificial time

derivatives are added to each equation, and an iterative block-implicit scheme [Ref. 12] is used. In prescribing no-slip boundary conditions, the tangential component (34) contains a contribution from ϕ; this contribution is evaluated using ϕ^n. Terms in the vorticity equation (A.1) containing u, v, w, v_ψ and w^ψ are evaluated using u^n, v^n, w^n, v^ψ and w^y; x-derivatives of v^ψ and w^ψ are evaluated using n- and (n-1)-level quantities, ω_1, ω_2, ω_3 are known and evaluated at n+1 level.

(2) The pressure equation (A.3) is solved for Δp^{n+1} using an iterative scalar ADI scheme. In this equation all appearances of v_ψ^{n+1} and w_y^{n+1} are evaluated using ψ^{n+1}, and u, v, w, ρ, v_ϕ and w_ϕ are evaluated using n-level quantities. r_1, r_2, r_3 and ω_1, ω_2, ω_3 are known and evaluated at n+1 level.

(3a) Using an assumed value of p_m^{n+1} to begin a secant iteration and values of Δp^n and Δp^{n+1} now available, the x-momentum equation (A.4) is solved to determine u^{n+1}, using a scalar ADI scheme.

(3b) The density ρ^{n+1} is evaluated from the state equation (A.5) using $\bar{U}^{n+1}$, p_m^{n+1} and Δp^{n+1}, which are now available.

(3c) For internal flows the integral mass-flux relation (37) is evaluated using u^{n+1} and ρ^{n+1}.

(3d) Assuming that the initial guess for p_m^{n+1} was not exact, the integral mass-flux relation will not be satisfied, and steps (3a-c) are repeated iteratively using the standard secant method [Ref. 13] to find the value of p_m^{n+1} that leads to u^{n+1} and ρ^{n+1} satisfying the integral mass-flux relation (37).

(4) Finally, the continuity equation (A.6) is solved for ϕ^{n+1} using an iterative scalar ADI scheme and currently available values of u^{n+1} and ρ^{n+1}. The velocity components v^{n+1}, w^{n+1}, v^{n+1} and w^{n+1} are then evaluated from ϕ^{n+1} and ψ^{n+1}.

COMPUTED RESULTS FOR ROTATING FLOWS

One of the motivations of the present study is the eventual computation of flow in centrifugal turbomachinery components such as centrifugal impellers. The treatment of radial impeller geometries requires that the present analysis

be generalized for use with nonorthogonal coordinate systems. This generalization and the implementation in impeller geometries is part of an ongoing investigation being performed under a related contract (DAAG29-85-C-0030). In the present study, the analysis is applied to rotating flows in simple geometries using orthogonal coordinates. The flows considered include laminar and turbulent flow in a rotating 90 degree bend with square cross section and turbulent flows in rotating straight pipes and ducts.

Laminar Flow in a Rotating 90 Degree Bend

The geometry and flow configuration considered are shown in Fig. 1. The flow enters the duct axially and leaves radially. The Reynolds number $Re = U_o D/\nu$ is 790, where U_o is the mean flow velocity, D is the duct width, and ν is kinematic viscosity. The duct has a square cross section, and the Mach number was taken as 0.001, which means that the flow considered is essentially incompressible. Both rotating and nonrotating flows are considered for this geometry. The initial boundary layer thickness δ_i/D was taken to be either 0.4 or 0.1. In Ref. 9, predictions for nonrotating flow with $\delta_i/D = 0.4$ were found to be in very good agreement with experimental measurements. For the rotating flow, two cases are reported here, one with Rossby number Ro equal to 5.0 and the other with Ro equal to 1.0. The Rossby number is defined as $Ro = U_o/2\Omega D$, where Ω is the rotation speed.

The small-scalar potential approximation is examined in Fig. 2 for both nonrotating flows and rotating flows with Ro = 1. The initial boundary layer thickness was 0.4. The maximum absolute value of each (ϕ or ψ) component of transverse velocity is shown against streamwise distance. The results in Fig. 2 show that the ϕ-component of the transverse velocity is significantly less than the ψ-component, except very near the entrance section of the bend. This comparison is taken as an indication that the assumption of small $\bar{U}_\phi$ is reasonable for these flows. The small-scalar potential approximation has proved adequate in all the test cases considered.

Computed results for both rotating and nonrotating flow cases with $\delta_i/D = 0.4$ are compared in Figs. 3-5. Shown in these figures are the transverse secondary-flow velocity vectors, the streamwise primary-flow velocity contours, and the static pressure contours for the flow at the 90 degree location, at the end of the bend. In the nonrotating flow, the curved duct

geometry generates a strong secondary flow as shown in Fig. 3, and this distorts the primary flow velocity as shown in Fig. 4. The static pressure is shown in Fig. 5. The rotating flow cases are also shown for comparison in Figs. 3-5. The Coriolis forces in the rotating flow exert an increasing influence on the flow development as the system rotation rate increases. The rotation causes additional secondary flow motion which tends to twist the counter-rotating vortices present in the nonrotating case, and this further distortion increases with increasing system rotation rate, as shown in Fig. 3. The streamwise velocity is shown in Fig. 4, and the observed distortion of the primary-flow velocity contours in the rotating flow case is consistent with the predicted secondary flow. Finally, the static pressure in Fig. 5 reflects a complicated interaction of the primary and secondary flows as influenced by duct curvature, centrifugal, and Coriolis force effects.

Fig. 6 and Fig. 7 show the effects of initial boundary layer thickness on the development of primary flow in both nonrotating and rotating 90 degree bends. The thicker boundary layer causes a stronger secondary flow which in turn generates stronger distortion in the primary flow as shown in Fig. 6 and Fig. 7. Physically, the secondary flow is generated inviscidly by the turning of transverse vorticity but its growth is retarded by viscous stress near walls. Viscous stresses exert a stronger retarding effect on thin boundary layer cases than on thick boundary layer cases. Thus, the thicker boundary layer flow generates stronger secondary flow and distortion in the primary flow. The computed effect of initial boundary layer on the development of primary and secondary flow is consistent with experimentally observed trends [Ref. 14].

Turbulent Flow in a Rotating 90 Degree Bend

The geometry and flow configuration are the same considered for laminar flow (Fig. 1). The flow parameters are Re = 50,000, Ro = 1.0 and initial shear layer thickness $\delta_i/D = 0.1$. This calculation was started in the straight extension upstream of the bend at a distance of 1.5 D from the start of the bend. The development of this flow at streamwise stations corresponding to 0, 30, 60 and 90 degrees of turning are shown in Figs. 8a-d. The development of the primary and secondary flow is shown in Figs. 8a-b. At the start of the bend (0 degrees) there is little Coriolis effect because the primary flow velocity is

parallel to the axis of rotation. There is only a small amount of secondary flow, and this is due to the effect of geometric curvature. As the bend angle of turning increases (30, 60, 90 degrees) there is an increased effect of Coriolis forces, combined with secondary flows generated by turning of the duct. The Coriolis forces cause additional secondary flow which twists the vortices induced by turning. The vortices migrate toward the forward wall in the direction of rotation (the low pressure surface) and this behavior is consistent with general experimental observations. A considerable amount of distortion of the primary flow is present, as is consistent with predicted secondary flows. Because the Coriolis force depends on the local flow speed, the overall flow structure is quite complicated. The secondary flow velocity is very large and of the same order of magnitude as the primary velocity in thin shear layers along the inside and outside walls of the bend. These large secondary vortices are the result of the primary flow momentum deficit in these shear layers subjected to Coriolis-induced pressure gradients.

The pressure coefficient for this flow is shown in Fig. 8c. At the start of the bend, the transverse pressure gradients are relatively mild. The gradient is essentially in the direction from outside to inside of the bend and is associated with geometric curvature effects. As the bend turning angle increases, the transverse pressure gradients gain considerable strength and are directed essentially in the direction of rotation with low pressure on the leading surface. Finally, contours of the streamwise pressure gradient ($\partial C_p/\partial x$) are shown in Fig. 8d. These gradients are of interest because the present analysis and governing equations were formulated to avoid approximations for this term in the primary flow momentum equation. These streamwise pressure gradients gain considerable strength and complexity with increasing bend turning angle; the transverse variation in this term is of order unity. It would be difficult to devise a pressure approximation for this term which would be adequate for rotating flow structures of this complexity.

Turbulent Flow in a Rotating Pipe

The geometry and flow configuration for this case are shown in Fig. 9. The Reynolds number $Re = U_m d/\nu$ is 6×10^4, based on pipe diameter, d, and mean axial velocity, U_m. The Rossby number $Ro = U_m/2\Omega d$ is 1.0, where Ω is the rate of rotation. The initial boundary layer thickness is 0.03 d, which was

estimated from the entrance axial velocity profile measured by Kikuyama, Murakami and Nishibori [Ref. 15] for these flow conditions. Kikuyama, Murakami and Nishibori [Ref. 15] measured time-mean velocity and turbulent fluctuations in this flow. They found the system rotation of the pipe has a stabilizing effect in the suppression of turbulence. Using the mixing-length theory, they suggested the following formulas for mixing length distribution to account for the suppression of the turbulence due to pipe rotation.

$$\ell/\ell_o = 1 - \beta Ri \tag{38}$$

where ℓ and ℓ_o denote the values of the mixing length for rotating and nonrotating flow. β is a constant, and R_i is the Richardson number defined by

$$Ri = \frac{2w}{r^2}\frac{\partial}{\partial r}(rw)\left\{\left(\frac{\partial u}{\partial z}\right)^2 + \left[r\frac{\partial}{\partial z}\left(\frac{w}{r}\right)\right]^2\right\} \tag{39}$$

Here, w is the swirl velocity and u is the streamwise velocity, r and z are distances from the center and the wall of pipes, respectively. In the present calculation, the mixing length distribution ℓ_o for nonrotating flow is computed by using equations (32), (33), and the mixing length distribution for turbulent pipe flow is calculated by using equations (38), (39). The coefficient, β, is chosen to be 2. The turbulent viscosity is obtained from equations (30), (31).

Figures (10a) and (10b) show a comparison of computed and measured streamwise velocity, u, and swirl velocity, w, components at station x/d = 28.8. The streamwise velocity, u, is normalized by free stream velocity, Ue, and the swirl velocity, w, is normalized by pipe radius, ro, and rotation rate, Ω. The distance from the pipe wall, r_o-r, is normalized by the momentum thickness, θx. The computed and measured velocity distributions are in good agreement.

Turbulent Flow in a Rotating Duct

The geometry and flow configuration for this test case are shown in Fig. 11. The rectangular cross section has a height to width ratio H/D = 0.368. The Reynolds number, Re, is 66,500, based on passage hydraulic diameter and mean velocity. The Rossby number, Ro, is 6, based on passage width, D, and mean

velocity. The initial boundary layer thickness used in the calculation is 0.05 D. The mixing length distribution from equation (32) was used for these calculations. In Figs. (12a) and (12b), the computed streamwise velocity in the horizontal center plane and secondary velocity in the vertical center plane are compared at x/D = 5 with the measurements of Wagner and Velkoff [Ref. 16] and the computed results of Howard, Patankar and Bordynuik [Ref. 7]. The present results agree very well with the measured streamwise velocity in Fig. (12a), and the improved agreement relative to the Ref. 7 calculation probably reflects the finer grid and resolution of the viscous sublayer region in the present results, compared with the wall-function treatment of Ref. 7. The comparison for secondary velocity in Fig. (12b) is less conclusive because of the difficulty of measuring small velocities near walls using hot wire anemometry.

CONCLUSIONS

A spatial marching analysis is described for computation of three-dimensional viscous flows with system rotation. The governing equations are based on a small scalar potential approximation for the secondary flow, which does not entail any approximation of the pressure gradient terms. The analysis was assessed by application to laminar and turbulent rotating flows in simple ducts and bends. This approach seems well suited for a number of rotating internal ducted flows at or near design conditions, and can provide very high resolution in three dimensions at relatively low costs. Adequate resolution of turbulent flows including viscous sublayer resolution appears to require at least 500,000 grid points even in the simple 90 degree bend geometry. Solutions obtained by the present method using 500,000 grid points require only about 15 minutes of CRAY-1S CPU time. Future work will address implementation of the analysis in nonorthogonal coordinates and computation of centrifugal impeller flows.

ACKNOWLEDGEMENT

The authors wish to thank Dr. Brian E. Thompson for valuable discussions relating to future development of this work in impeller geometries.

Proposal Number 19149-EG

Funding Document DAAG29-82-C-0021

Publications: Numerical Study of Three-Dimensional Viscous Flows with System Rotation, S.J. Lin, W.R. Briley and H. McDonald, AIAA Paper No. 85-1691, 18th Fluid Dynamics and Plasmadynamics and Lasers Conference, 1985.

Participating Personnel: H. McDonald, W.R. Briley, S.J. Lin
T.R. Govindan, R. Levy, B.E. Thompson

REFERENCES

1. Patankar, S.V., Spalding, D.B.: A Calculation Procedure for Heat, Mass, and Momentum Transfer in Three-Dimensional Parabolic Flows, Intl. J. Heat Mass Transfer, Vol. 15, pp. 1787-1805, 1972.

2. Caretto, L.S., Curr, R.M. and Spalding, D.B.: Two Numerical Methods for Three-Dimensional Boundary Layers, Comp. Meth. Appl. Mech and Eng., Vol. 1, pp. 39-57, 1973.

3. Briley, W.R.: Numerical Method for Predicting Three-Dimensional Steady Viscous Flow in Ducts, J. Comp. Phys., Vol 34, pp. 54-73, 1974.

4. Ghia, K.N. and Sokhey, J.S.: Laminar Incompressible Viscous Flow in Curved Ducts of Regular Cross-Section, Trans. ASME, J. Fluids Eng., Vol. 99, pp. 640-648, 1977.

5. Kreskovsky, J.P., Briley, W.R and McDonald, H.: Analysis and Computation of Three-Dimensional Flow in Strongly Curved Ducts in Computer in Flow Predictions and Fluid Dynamics Experiments, ASME, pp. 129-140, 1981.

6. Levy, R., Briley, W.R and McDonald, H.: Viscous Primary/Secondary Flow Analysis for Use With Nonorthogonal Coordinate Systems, AIAA paper 83-0556, 1983.

7. Howard, J.H.G., Patankar, S.V. and Bordynuik, R.M.: Flow Prediction in Rotating Ducts Using Coriolis-Modified Turbulence Models, J. of Fluids Eng., Vol. 102, pp. 456-461.

8. Majumdar, A.K., Pratap, V.S. and Spalding, D.B.: Numerical Computation of Flow in Rotating Ducts, J. of Fluids Eng., pp. 148-153, March, 1977.

9. Briley, W.R. and McDonald, H.: Three-Dimensional Viscous Flows with Large Secondary Velocity, J. Fluid Mech., Vol 144, pp. 47-77, 1984.

10. Lin, S.J., Briley, W.R. and McDonald, H.: Numerical Study of Three-Dimensional Viscous Flows with System Rotation, AIAA Paper 85-1691, 1985.

11. McDonald, H. and Camarata, F.J.: An Extended Mixing Length Approach for Computing the Turbulent Boundary-Layer Development, In Proceedings, Stanford Conf. of Turbulent Boundary Layers, Vol. I, Pub. by Stanford Univ., pp. 83-98, 1969.

12. Briley, W.R. and McDonald, H.: On the Structure and Use of Linearized Block ADI and Related Schemes, J. Comp. Phys., Vol. 34, pp. 54-73.

13. Ralston, A.: A First Course in Numerical Analysis, McGraw-Hill, 1965.

14. Taylor, A.M.K.P., Whitelaw, J.H., Yianneskis, M.: Curved Ducts With Strong Secondary Motion: Velocity Measurements of Developing Laminar and Turbulent Flow, J. of Fluids Eng., Vol. 104, pp. 350-359, 1982.

15. Kikuyama, K., Murakami, M. and Nishibori, K.: Development of Three-Dimensional Turbulent Boundary Layer in an Axially Rotating Pipe, J. of Fluids Eng., Vol. 105, pp. 154-160, 1983.

16. Wagner, R.E. and Velkoff, H.R.: Measurements of Secondary Flows in a Rotating Duct, J. of Eng. for Power, pp. 261-270, 1972.

APPENDIX A

Governing Equations in Rotating Orthogonal Coordinates

The governing equations for the reduced form of the Navier-Stokes equations based on the small-scalar potential approximation is given below in a general rotating orthogonal coordinate system.

Vorticity Equation

$$
\begin{aligned}
&\frac{\rho u}{h_1}\frac{\partial}{\partial x}h_2h_3\Omega_1 + \frac{\partial}{\partial y}h_3\rho v\Omega_1 + \frac{\partial}{\partial z}h_2\rho w\Omega_1 \\
&+ \frac{\partial h_3\tilde{w}}{\partial x}\frac{\partial}{\partial y}\left(\frac{\rho u}{h_1}\right) - \frac{\partial h_2\tilde{v}}{\partial x}\frac{\partial}{\partial z}\left(\frac{\rho u}{h_1}\right) - \frac{\partial}{\partial y}(h_3\rho u^2K_{13}) \\
&+ \frac{\partial}{\partial z}(h_2\rho u^2K_{12}) + \frac{\partial\rho v}{\partial y}\frac{\partial\tilde{v}}{\partial z} - \frac{\partial\rho v}{\partial z}\frac{\partial\tilde{v}}{\partial y} \\
&+ \frac{\partial\rho w}{\partial y}\frac{\partial\tilde{w}}{\partial z} - \frac{\partial\rho w}{\partial z}\frac{\partial\tilde{w}}{\partial y} \\
&= \left[\frac{\partial}{\partial y}\frac{h_3}{h_1h_2}\frac{\partial}{\partial y} + \frac{\partial}{\partial z}\frac{h_2}{h_1h_3}\frac{\partial}{\partial z}\right](\mu+\mu_T)h_1\Omega_1 \\
&- 2\frac{\partial}{\partial y}\left[\rho h_3(\omega_1v - \omega_2u)\right] + 2\frac{\partial}{\partial z}\left[\rho h_2(\omega_3u - \omega_1w)\right]
\end{aligned}
\tag{A.1}
$$

Here, Ω_1 is streamwise vorticity, and ω_1, ω_2, ω_3 are components of the system rotation-rate vector. K_{ij} is given in equation (16).

Vorticity Definition

$$
\frac{\partial}{\partial y}\left(\frac{h_3}{h_1h_2}\frac{1}{\rho}\frac{\partial h_1\psi}{\partial y}\right) + \frac{\partial}{\partial z}\left(\frac{h_2}{h_1h_3}\frac{1}{\rho}\frac{\partial h_1\psi}{\partial z}\right) = -h_2h_3\Omega_1 \tag{A.2}
$$

Pressure Equation

$$\left[\frac{\partial}{\partial y}\frac{h_1h_3}{h_2}\frac{\partial}{\partial y}+\frac{\partial}{\partial z}\frac{h_1h_2}{h_3}\frac{\partial}{\partial z}\right](P+\Delta p)+\frac{\partial}{\partial y}h_1h_3\rho\tilde{C}_2$$

$$+\frac{\partial}{\partial z}h_1h_2\rho\tilde{C}_3+2\frac{\partial}{\partial y}\left[\rho h_1h_3(\omega_3u-\omega_1w)\right] \qquad (A.3)$$

$$+2\frac{\partial}{\partial z}\left[\rho h_1h_2(\omega_1v-\omega_2u)\right]+\frac{\partial}{\partial y}\left\{\rho h_1h_3\left[\omega_3(\omega_2r_3-\omega_3r_2)-\omega_1(\omega_1r_2-\omega_2r_1)\right]\right\}$$

$$+\frac{\partial}{\partial z}\left\{\rho h_1h_2\left[\omega_1(\omega_3r_1-\omega_1r_3)-\omega_2(\omega_2r_3-\omega_3r_2)\right]\right\}=0 \quad .$$

where $\tilde{C}_2$ and $\tilde{C}_3$ are given in equations (17), (18), and r_1, r_2, r_3 are components of the position vector.

x-Momentum

$$\frac{u}{h_1}\frac{\partial u}{\partial x}+\frac{v}{h_2}\frac{\partial u}{\partial y}+\frac{w}{h_3}\frac{\partial u}{\partial z}+u(vK_{12}+wK_{13})$$

$$-v^2K_{21}-w^2K_{31}+(\rho h_1)^{-1}\partial(P+p_m+\Delta p)/\partial x$$

$$-\omega_2(\omega_1r_2-\omega_2r_1)+\omega_3(\omega_3r_1-\omega_1r_3)-2(\omega_2w-\omega_3v) \qquad (A.4)$$

$$=(\rho J)^{-1}\left[\frac{\partial}{\partial y}\frac{h_1^2h_3}{h_2}(\mu+\mu_T)\frac{\partial}{\partial y}\left(\frac{u}{h_1}\right)+h_1^2h_3(\mu+\mu_T)K_{12}\right.$$

$$\left.\frac{\partial}{\partial y}\left(\frac{u}{h_1}\right)+\frac{\partial}{\partial z}\frac{h_1^2h_2}{h_3}(\mu+\mu_T)\frac{\partial}{\partial z}\left(\frac{u}{h_1}\right)+h_1^2h_2(\mu+\mu_T)K_{13}\frac{\partial}{\partial z}\left(\frac{u}{h_1}\right)\right]$$

where $J = h_1h_2h_3$

State Equation

$$P + \rho_m + \Delta p = \frac{\gamma - 1}{\gamma} \rho \left(E_o - \frac{\bar{U} \cdot \bar{U}}{2} \right) \tag{A.5}$$

Continuity

$$\frac{\partial}{\partial x} (h_2 h_3 \rho u) + \frac{\partial}{\partial y} \rho \frac{h_1 h_3}{h_2} \frac{\partial \phi}{\partial y} + \frac{\partial}{\partial z} \rho \frac{h_1 h_2}{h_3} \frac{\partial \phi}{\partial z} = 0 \tag{A.6}$$

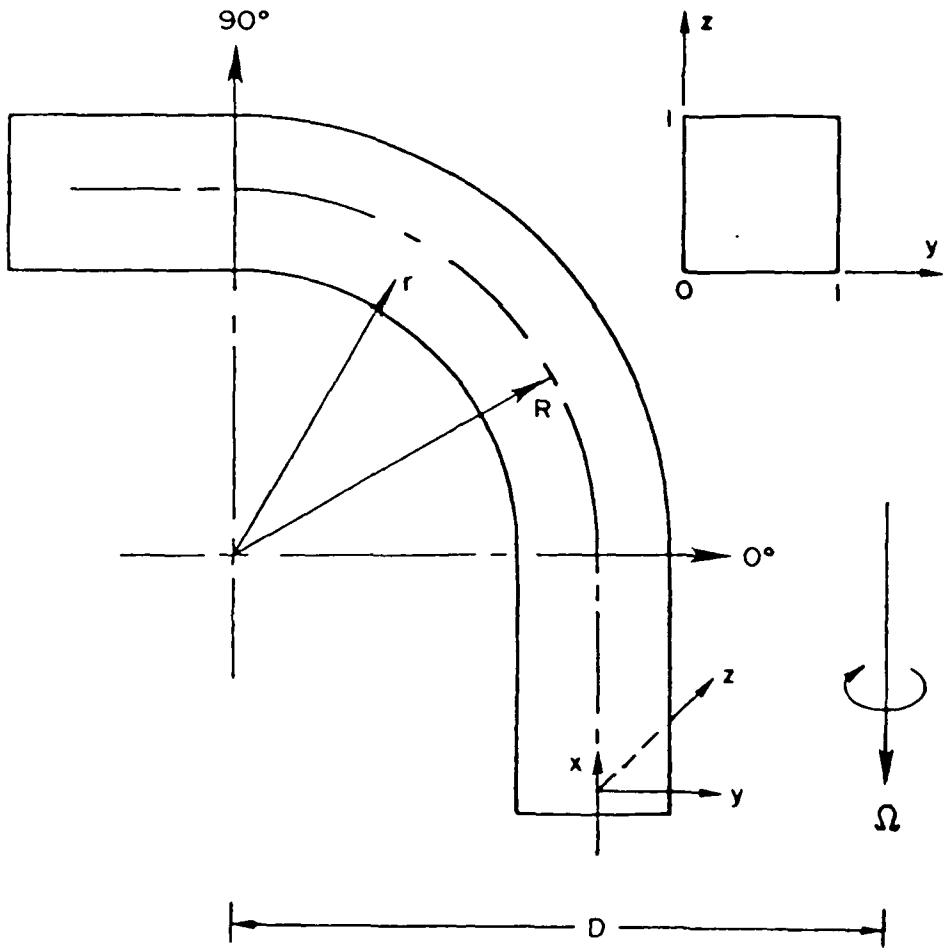

Figure 1- Rotating Flow in 90° Bend.

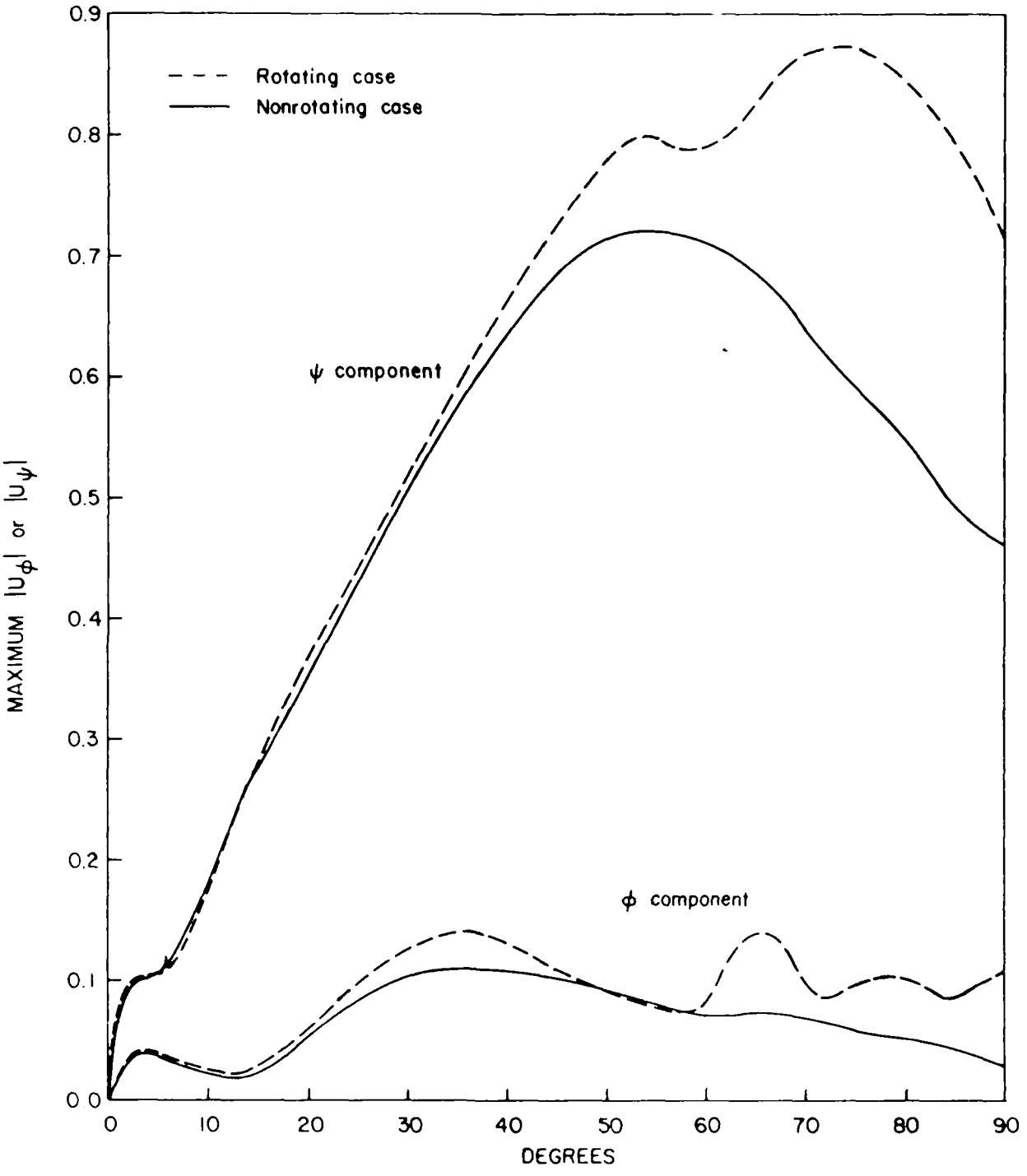

Figure 2 - Validation of the Small-Scalar-Potential Approximation for flow in a 90° Bend.

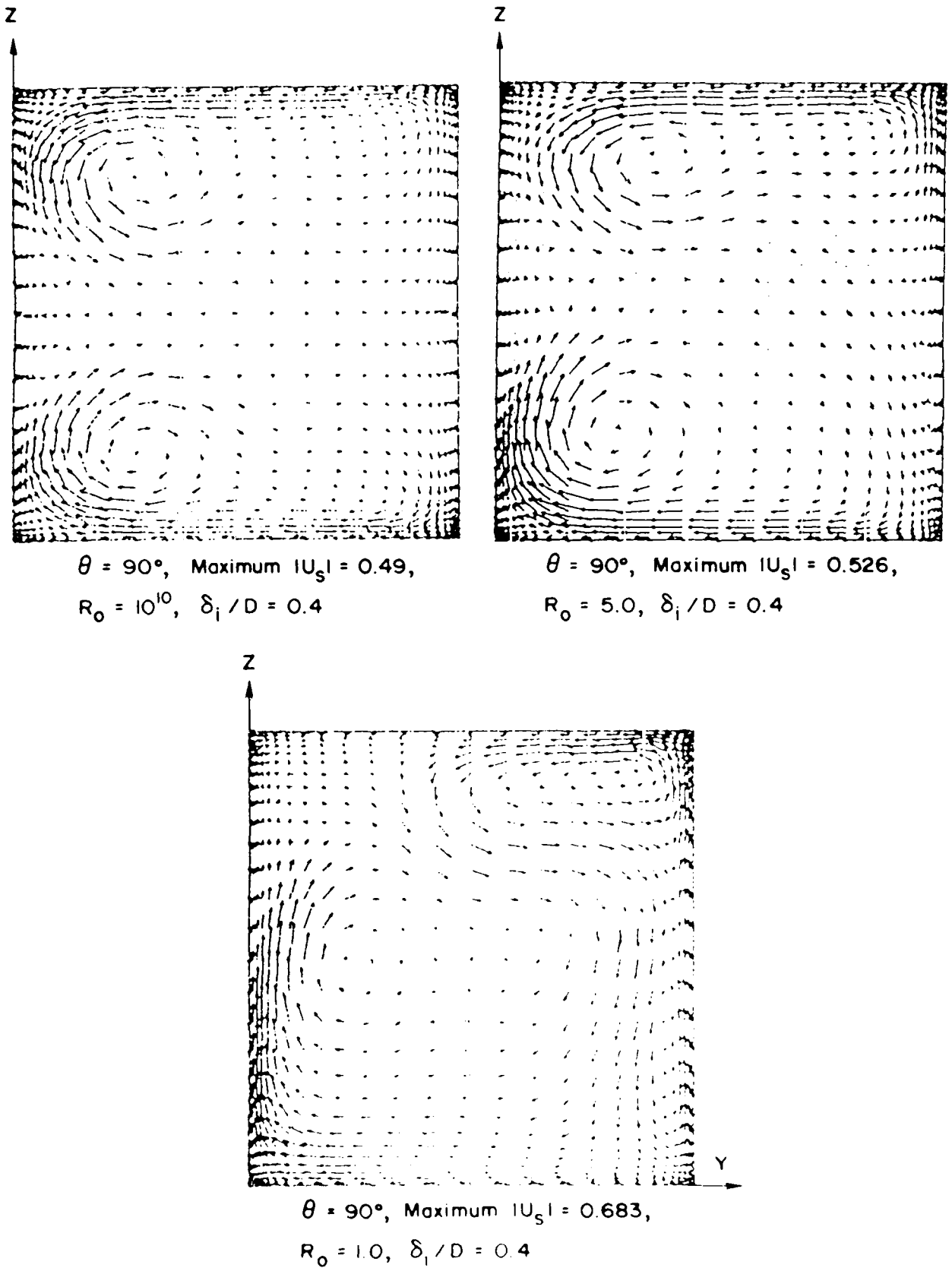

θ = 90°, Maximum $|U_s|$ = 0.49,
$R_o = 10^{10}$, δ_i / D = 0.4

θ = 90°, Maximum $|U_s|$ = 0.526,
R_o = 5.0, δ_i / D = 0.4

θ = 90°, Maximum $|U_s|$ = 0.683,
R_o = 1.0, δ_i / D = 0.4

Figure 4 - Effect of Rotation Rate on Secondary Flow in a 90° Bend

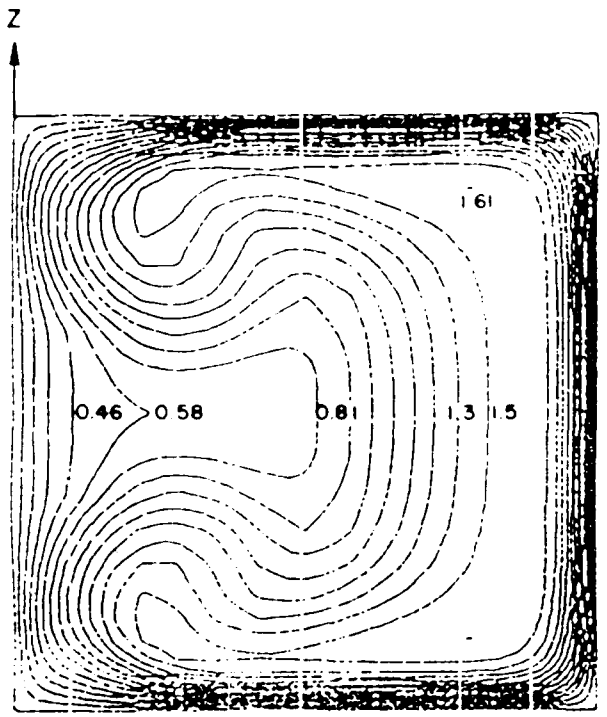

θ = 90°, Maximum $|\bar{U}_p|$ = 1.61,

$R_o = 10^{10}$, δ_i / D = 0.4

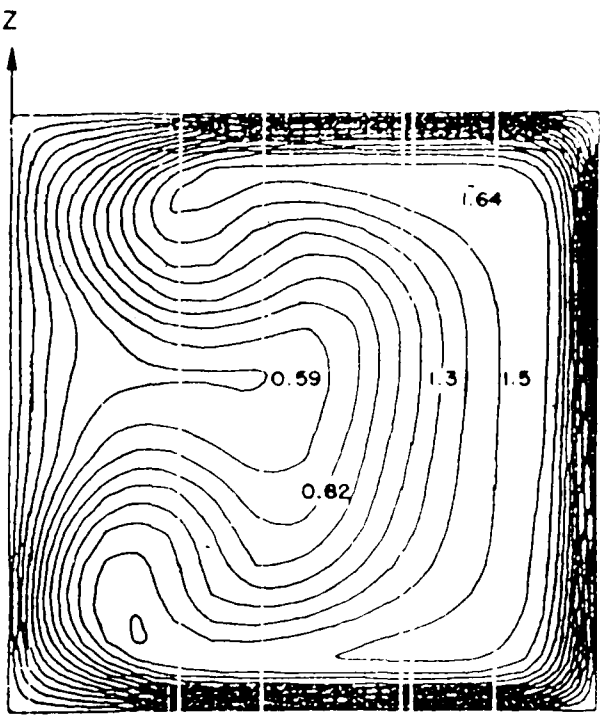

θ = 90°, Maximum $|\bar{U}_p|$ = 1.64,

R_o = 5.0, δ_i / D = 0.4

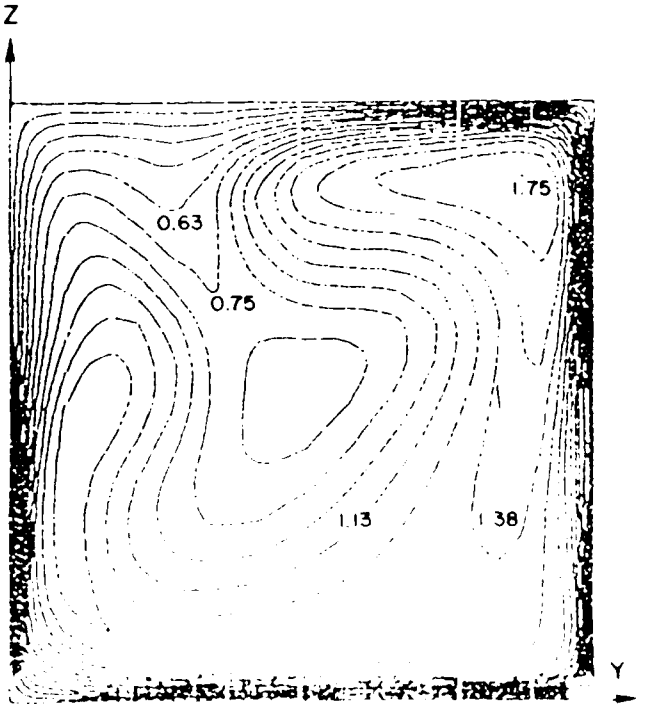

θ = 90°, Maximum $|\bar{U}_p|$ = 1.753,

R_o = 1.0, δ_i / D = 0.4

Figure 4 Effect of Rotation on Primary Flow [illegible]

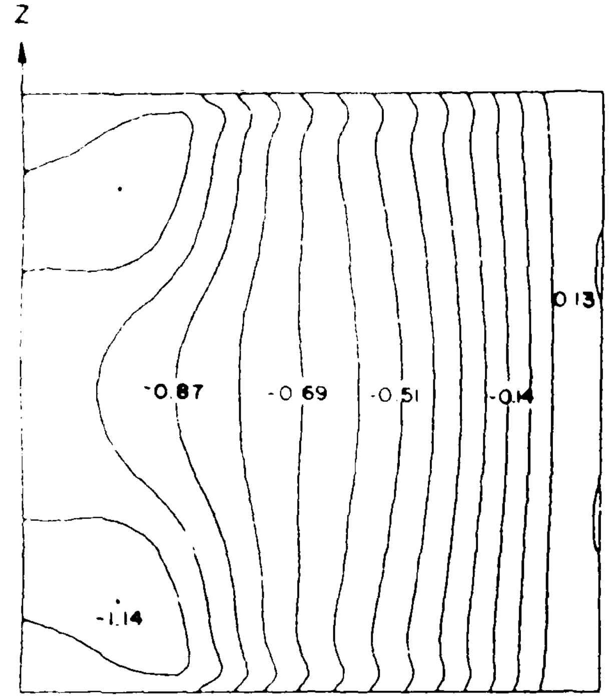

Maximum C_p = 0.13, Minimum C_p = −1.14,
θ = 90°, R_o = 10^{10}, δ_i/D = 0.4

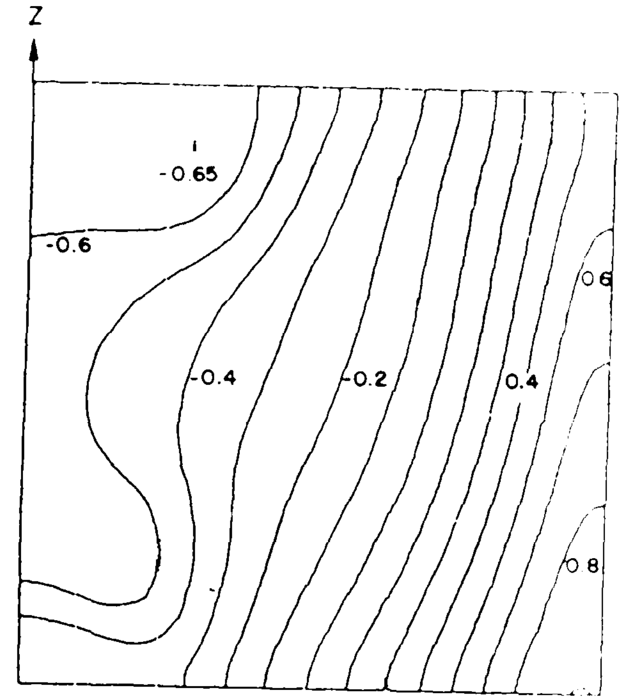

Maximum C_p = 0.877, Minimum C_p = −0.651,
θ = 90°, R_o = 5.0, δ_i/D = 0.4

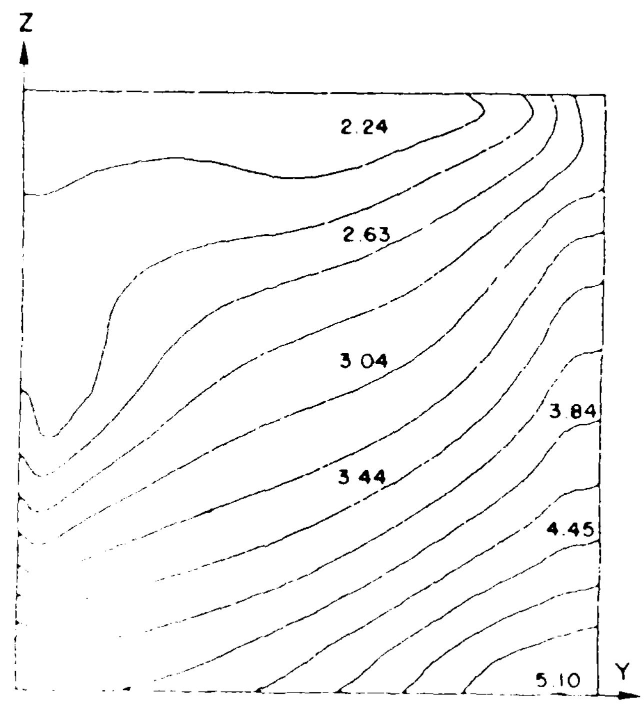

Maximum C_p = 5.1, Minimum C_p = 2.24,
θ = 90°, R_o = 1.0, δ_i/D = 0.4

Figure [illegible]. Effect of Rotation Rate on Static Pressures in a 90° Bend.

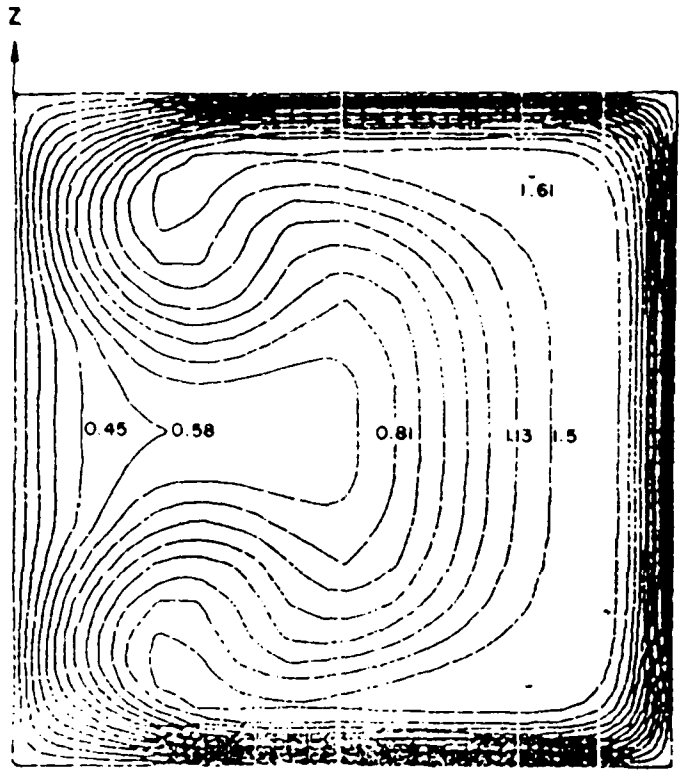

$\theta = 90°$, Maximum $|\bar{U}_p| = 1.61$, $R_0 = 10^{10}$, $\delta_1/D = 0.4$

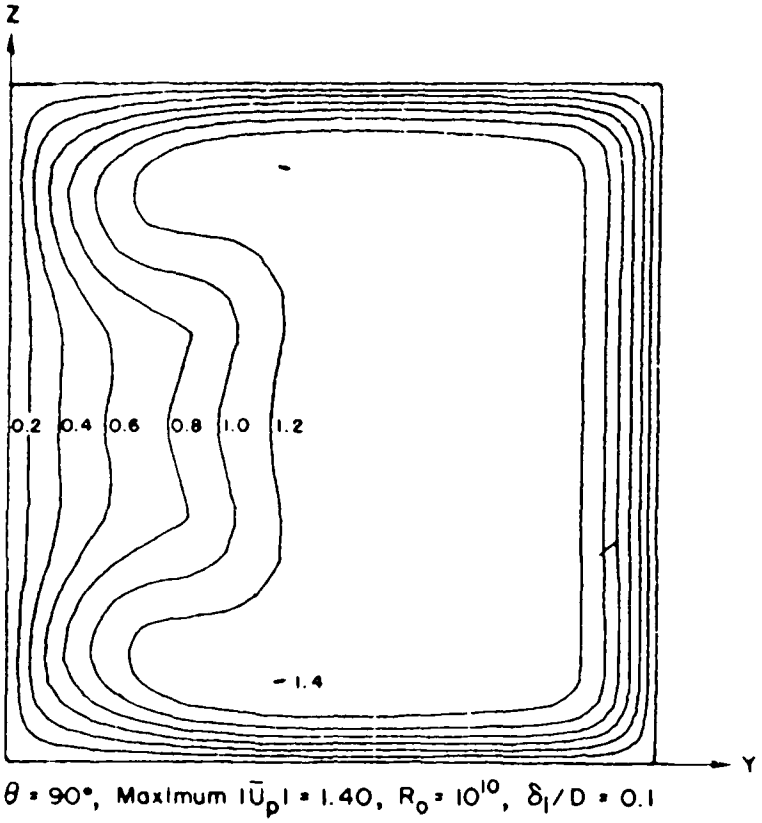

$\theta = 90°$, Maximum $|\bar{U}_p| = 1.40$, $R_0 = 10^{10}$, $\delta_1/D = 0.1$

Figure 6 - Effect of Initial Boundary Layer Thickness on Primary Flow in a Nonrotating 90° Bend.

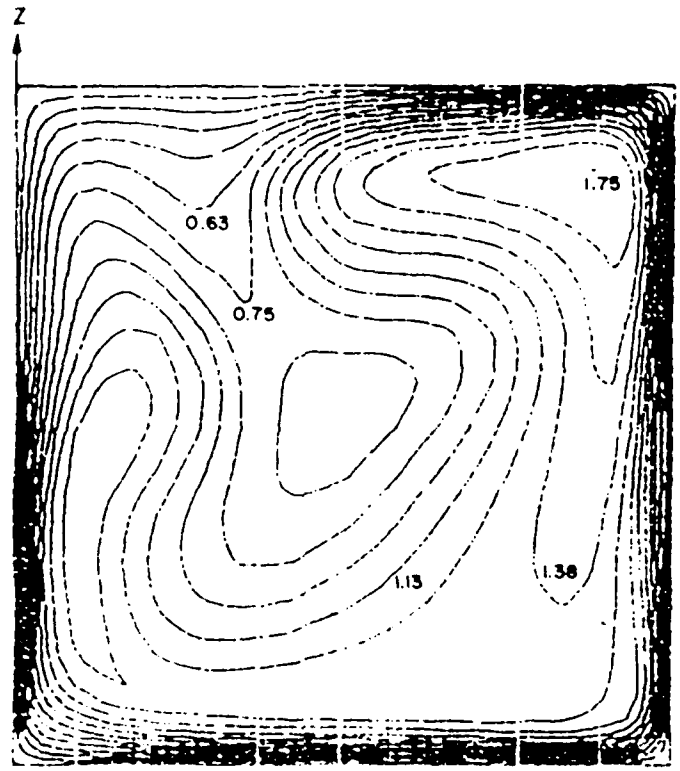

θ = 90°, Maximum $|\bar{U}_p|$ = 1.753, R_o = 1.0, δ_i/D = 0.4

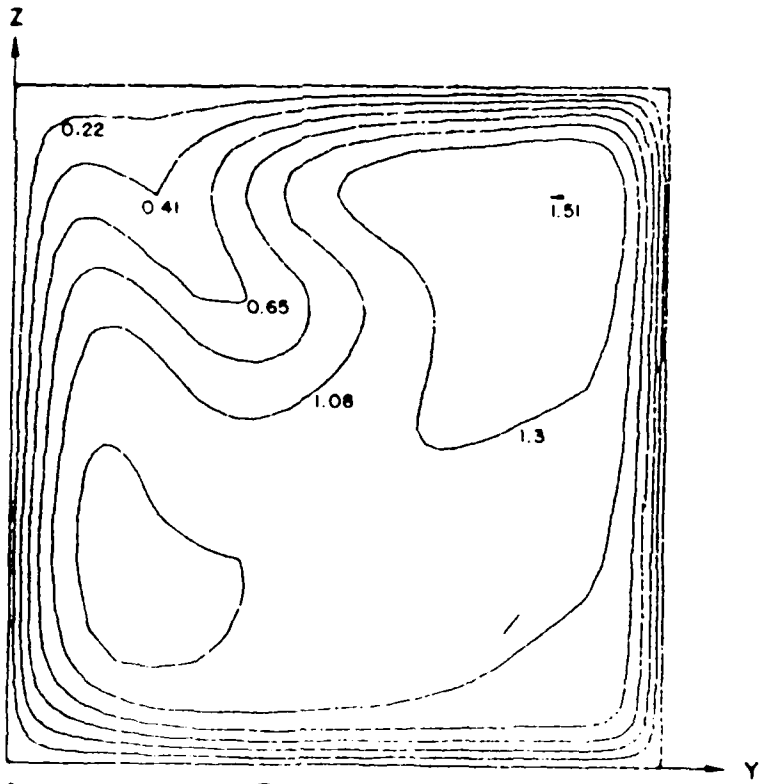

θ = 90°, Maximum $|\bar{U}_p|$ = 1.51, R_o = 1.0, δ_i/D = 0.1

Figure 7 - Effect of Initial Boundary Layer Thickness on Primary Flow in a Rotating 90° Bend.

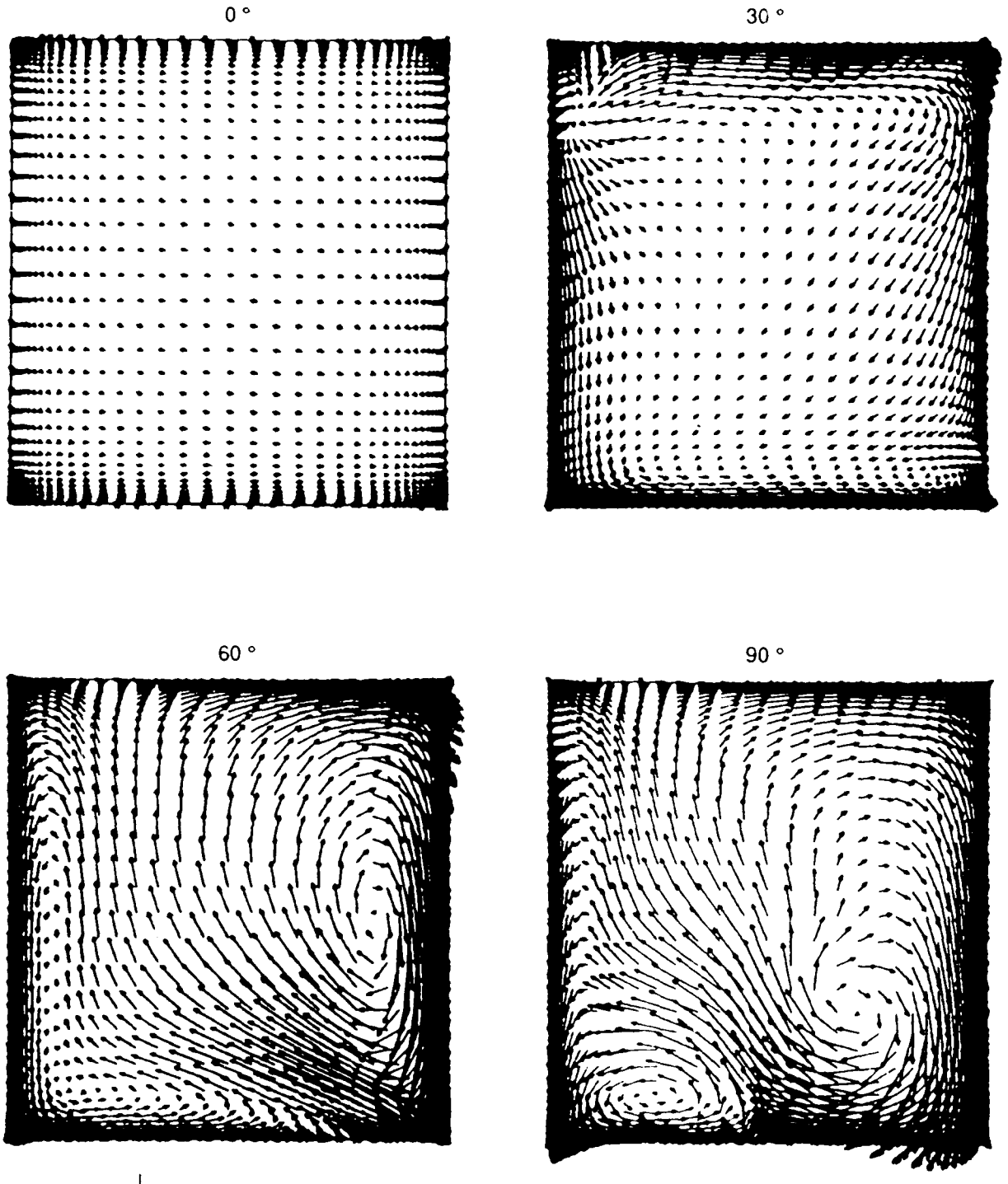

Figure 8a - Development of Secondary Flow Velocity Vectors for Turbulent Flow in a Rotating 90° Bend.

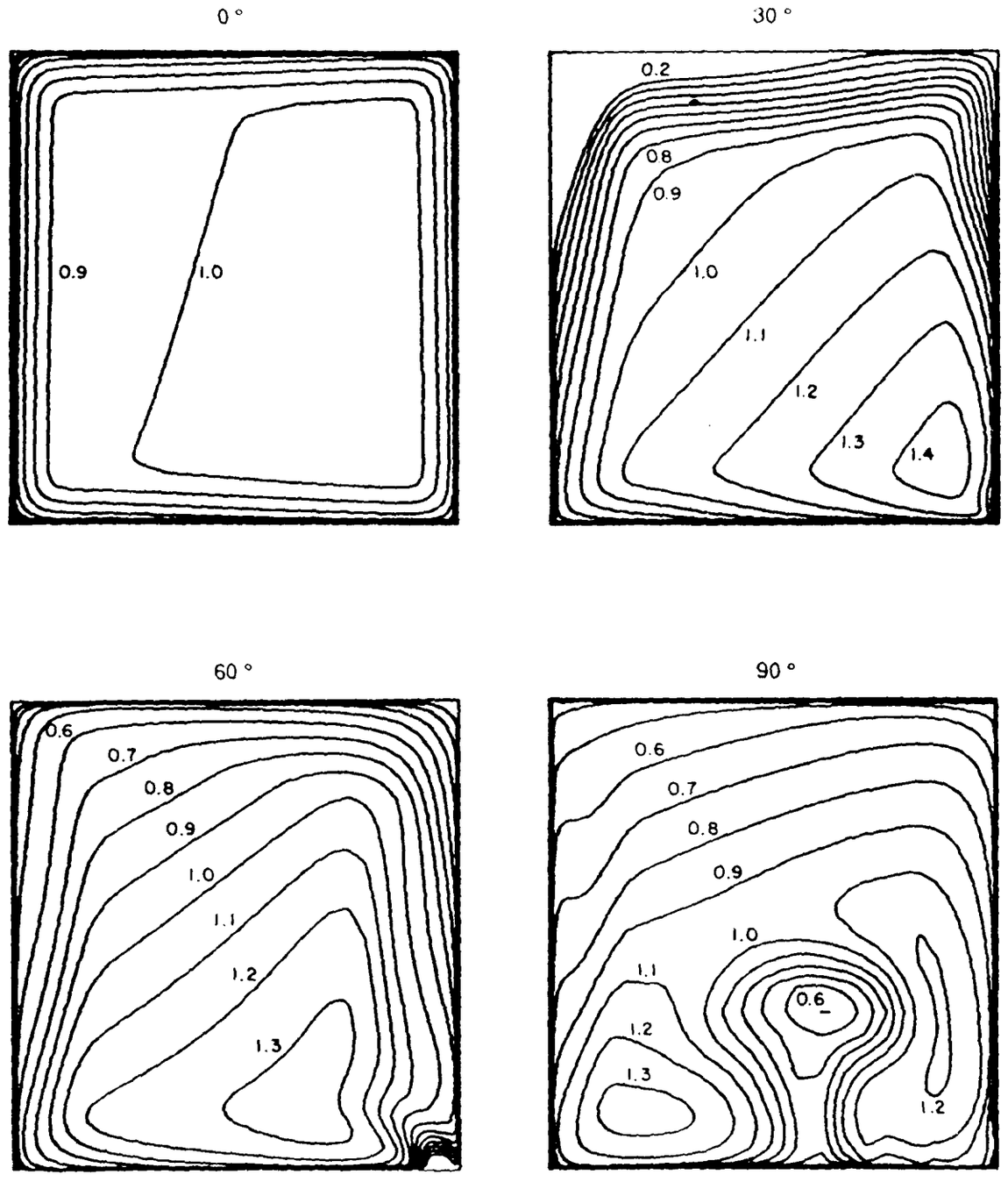

Figure 8b - Development of Primary Flow Velocity Contours for Turbulent Flow in a Rotating 90° Bend.

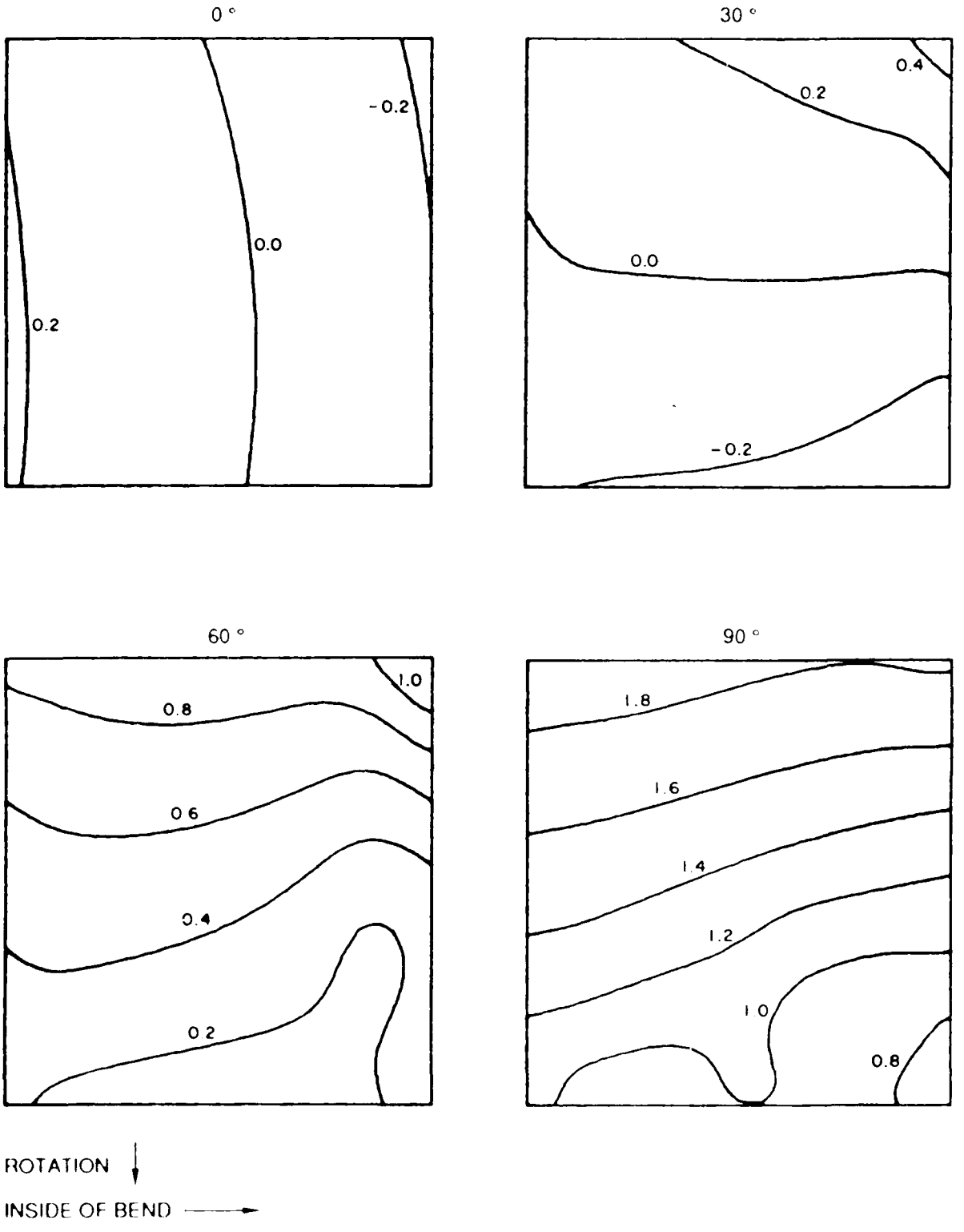

Figure 8c - Development of Pressure Coefficient Contours for Turbulent Flow in a Rotating 90° Bend.

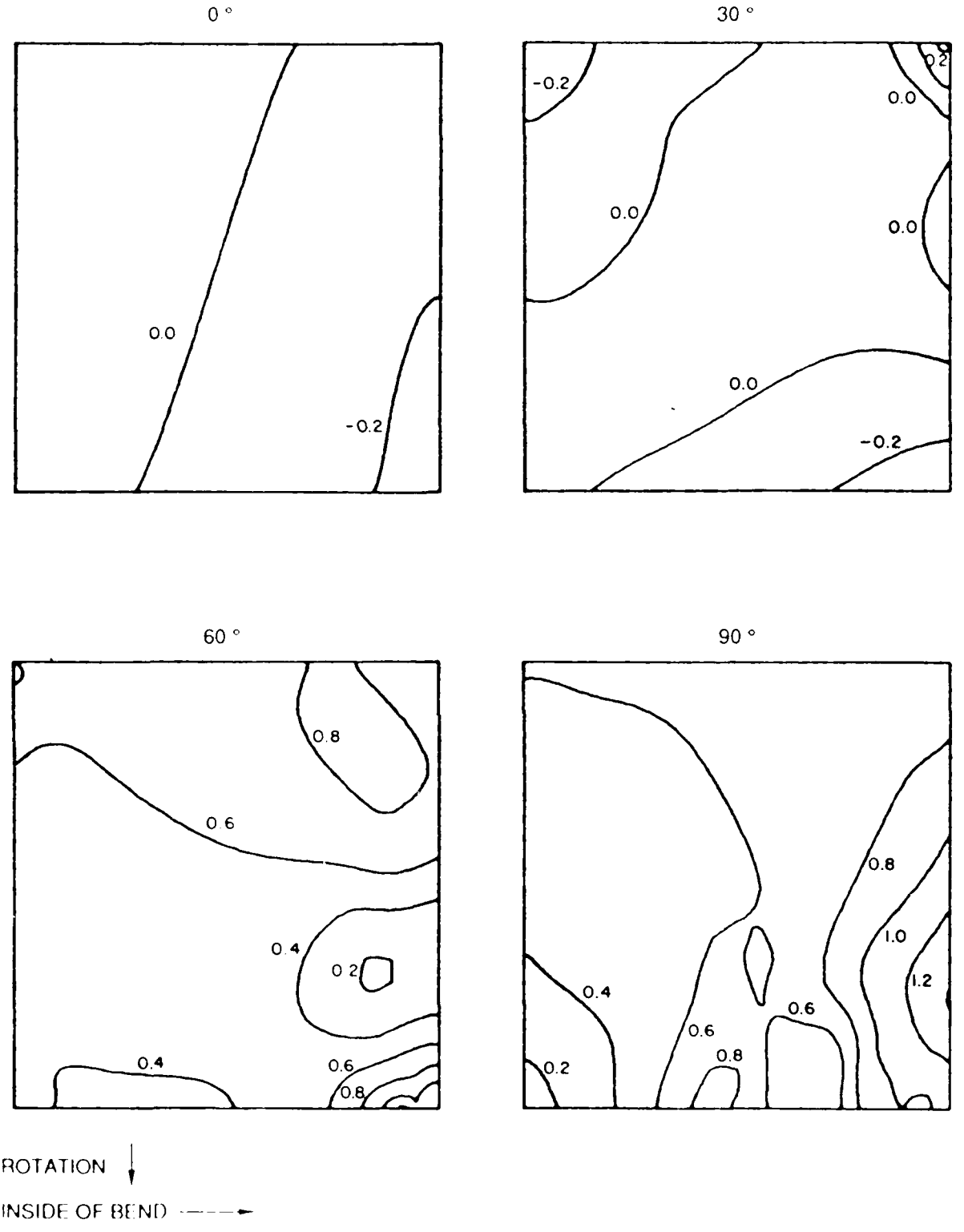

Figure 8d - Development of Streamwise Pressure Gradient $d(C_p)/dx$ Contours for Turbulent Flow in a Rotating 90° Bend.

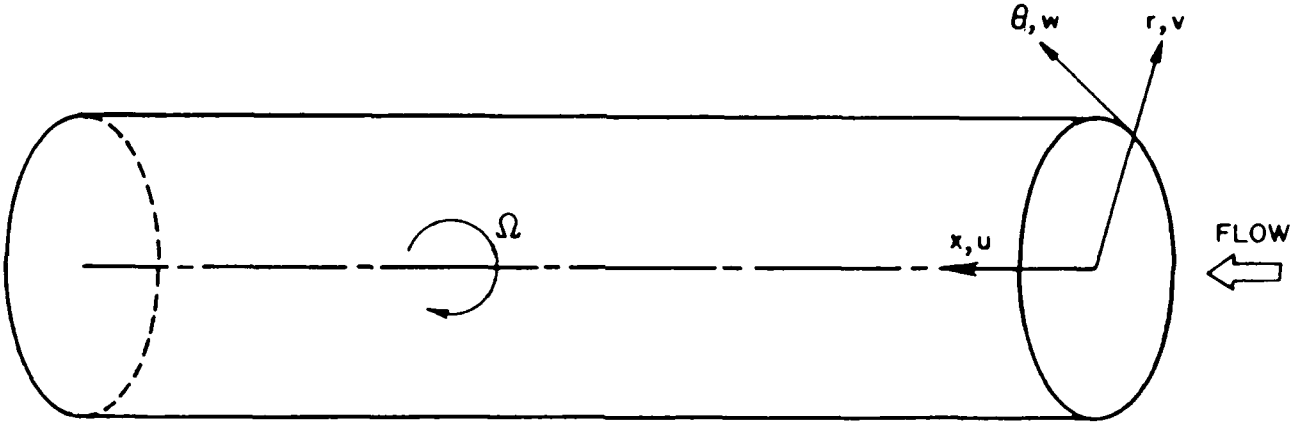

Figure 9 - Geometry for Rotating Flow in a Pipe.

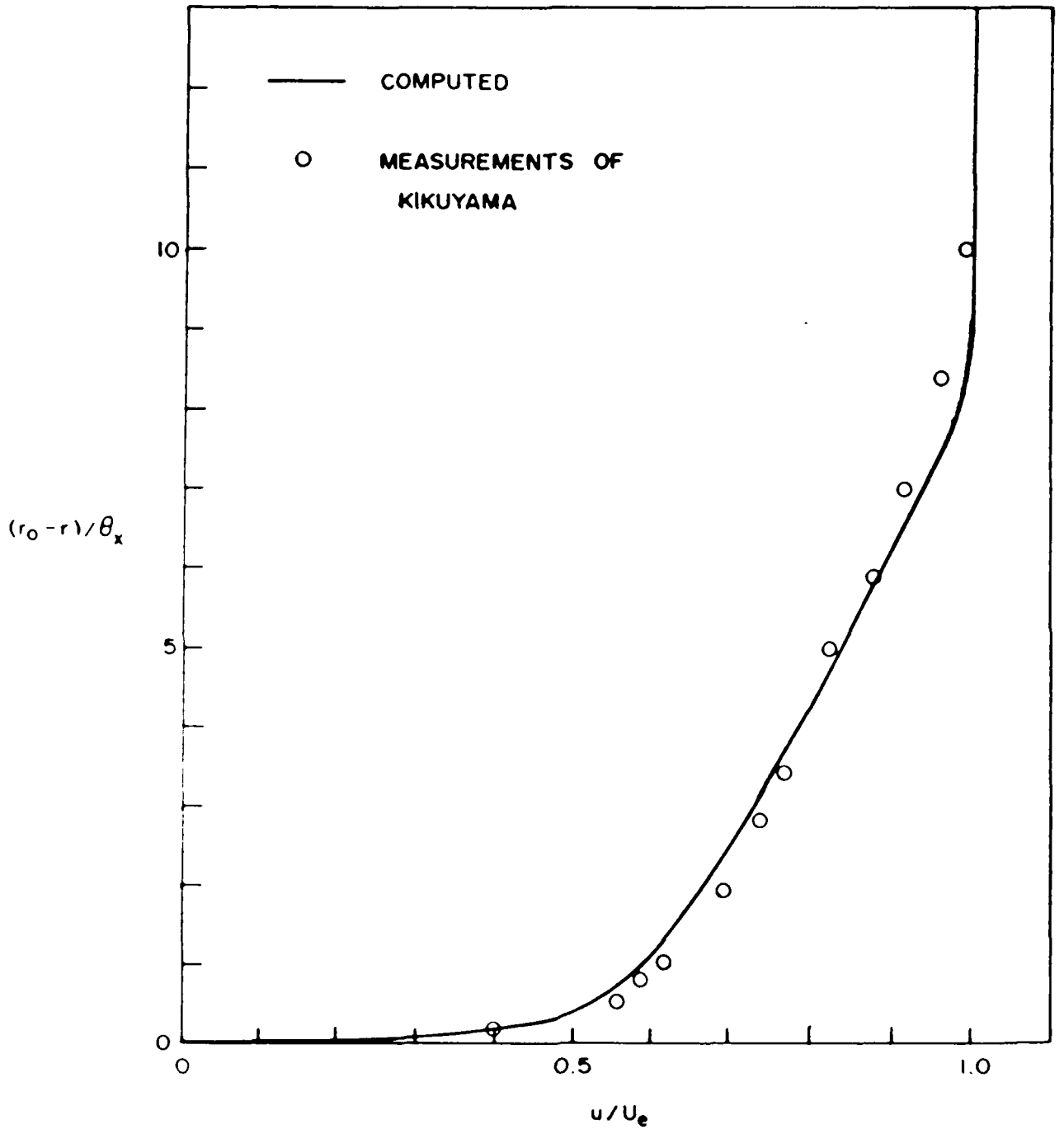

Figure 10a - Streamwise Velocity Profile at Station X/D = 28.8, R = 1.0, $Re = 6 \times 10^5$.

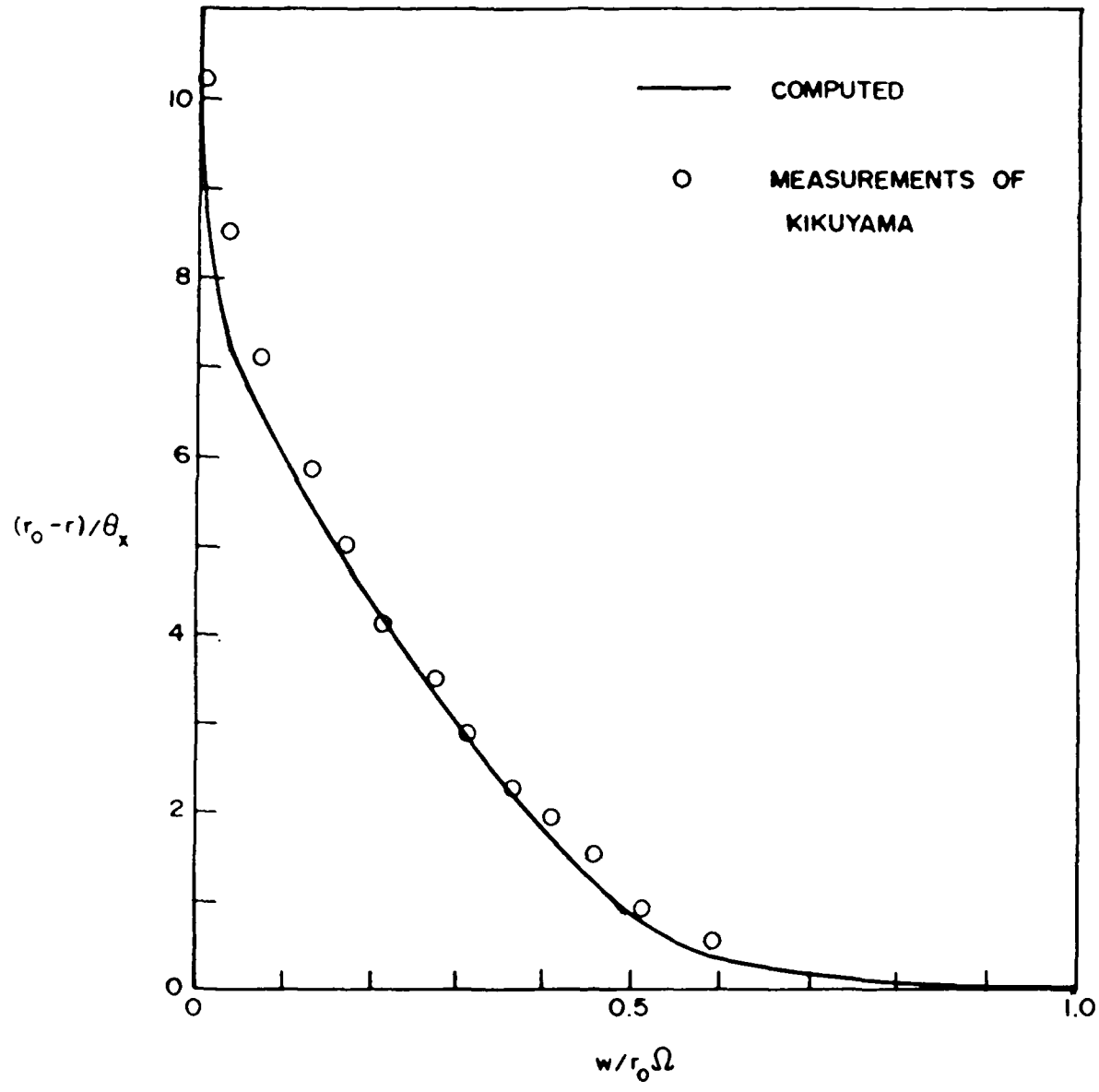

Figure 10b - Transverse Velocity Profile at Station X/D = 28.8, R_0 = 1.0, Re = 6 x 10^4.

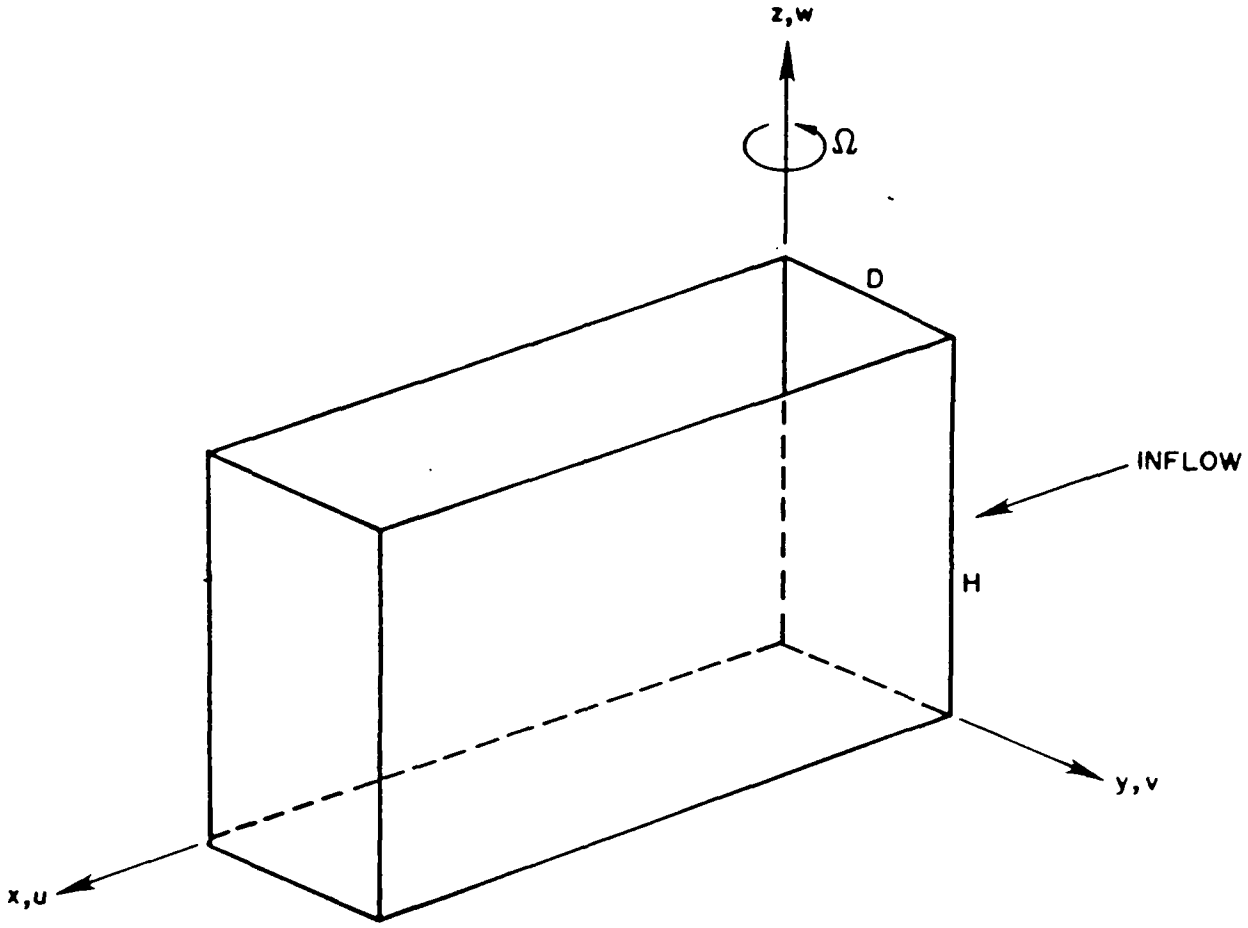

Figure 11 - Geometry for Rotating Flow in a Straight Duct.

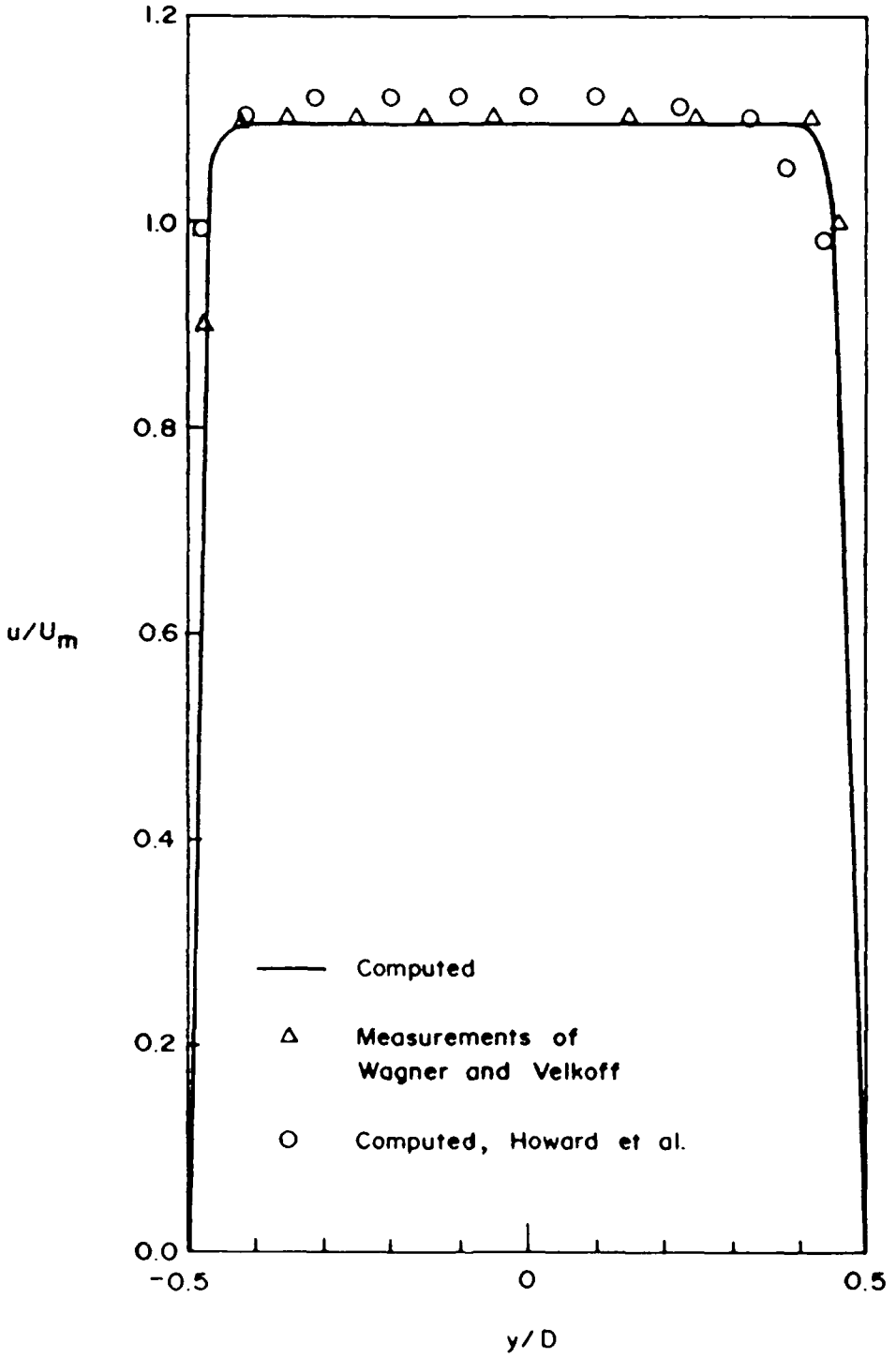

Figure 12a - Streamwise Velocity Profile at Station X/D = 5.0, R_0 = 6.0, Re = 6.65×10^4.

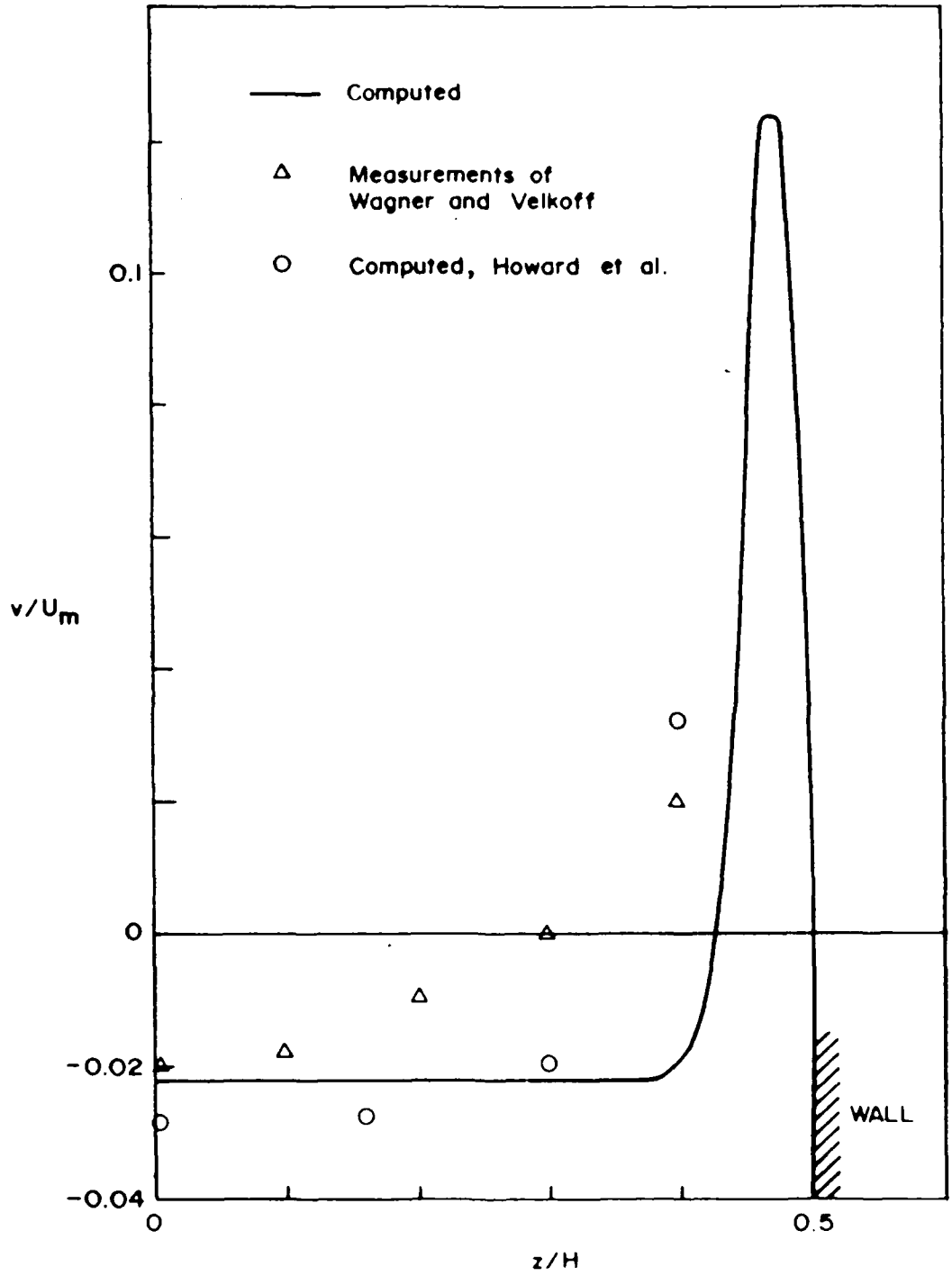

Figure 12b - Secondary Velocity Profile at Station X/D = 5.0, R = 6.0, Re = 6.65 x 10^6

END

3-87

DTIC